ANL-77-69

PHYSICS OF REACTOR SAFETY

Quarterly Report
April–June 1977

ARGONNE NATIONAL LABORATORY, ARGONNE, ILLINOIS

Prepared for the U. S. NUCLEAR REGULATORY COMMISSION
under Contract W-31-109-Eng-38

Printed in the United States of America
Available from
National Technical Information Service
U. S. Department of Commerce
5285 Port Royal Road
Springfield, Virginia 22161
Price: Printed Copy $4.50; Microfiche $3.00

Distribution Category:
Advanced Reactor Safety
Research—Fast Reactors
(NRC-7)

ANL-77-69

ARGONNE NATIONAL LABORATORY
9700 South Cass Avenue
Argonne, Illinois 60439

PHYSICS OF REACTOR SAFETY

Quarterly Report
April—June 1977

Applied Physics Division

September 1977

Work performed for the
Division of Reactor Safety Research
U. S. Nuclear Regulatory Commission

Previous reports in this series

ANL-76-114	April—June 1976
ANL-77-9	July—September 1976
ANL-77-22	October—December 1976
ANL-77-48	January—March 1977

TABLE OF CONTENTS

LIST OF FIGURES

LIST OF FIGURES (Contd)

LIST OF TABLES

PHYSICS OF REACTOR SAFETY

Quarterly Report
April-June 1977

ABSTRACT

This quarterly progress report summarizes work done in Argonne National Laboratory's Applied Physics Division and components Technology Division for the Division of Reactor Safety Research of the U. S. Nuclear Regulatory Commission during the months of April-June 1977. The work in the Applied Physics Division includes reports on reactor safety program by members of the Reactor Safety Appraisals Group, Monte Carlo analysis of safety-related critical assembly experiments by members of the Theoretical Fast Reactor Physics Group, and planning of safety-related critical experiments by members of the Zero Power Reactor (ZPR) Planning and Experiments Group. Work on Reactor core thermal-hydraulic code development performed in the Components Technology Division is also included in this report.

I. TECHNICAL COORDINATION - FAST REACTOR SAFETY ANALYSIS (A2015)

A. Summary

HCDA calculations have been carried out in which FX2-POOL was coupled to USEFUL, a code which calculates penetration of a molten fuel-steel mixture through a pin bundle. Heat transfer to steel cladding above the core was found to reduce fuel expansion work greatly.

A methodology has been developed for dealing with fluctuating parameters in an HCDA such as droplet or particle size. Representative distribution functions are selected for the fluctuating parameters, and these functions are sampled randomly in the course of the calculation. Although the distribution functions may not actually be known, reasonable bounding assumptions can be made for them which result in a significant reduction in the effect of variation in a fluctuating parameter compared to the usual assumption of various fixed values for the parameter. The new methodology has been applied to fuel particle sizes in fuel-steel heat transfer calculations with FX2-POOL and to FCI calculations with EPIC.

A fuel vapor ejection model has been included in EPIC. This model, which includes fuel vapor condensation in the coolant channel, will be particularly useful for failure of fresh fuel pins in which fission gas is not present.

The EPIC parameter studies have been completed. Extreme sensitivity of reactivity insertion to failure location was found, consistent with earlier studies. Increasing rip length had a mitigating effect on fuel reactivity insertion because fuel motion in the pin to the failure locations has an increasingly negative effect. For an 80% voided channel results for increasing rip length did not vary greatly from those for a single node failure.

A new technique has been developed for dealing with the numerical difficulty associated with the overcompaction of single-phase regions in fast reactor HCDA calculations. In this method, if overcompaction is occurring the divergence of the liquid velocity is set equal to the time rate of formation of excess liquid volume fraction. Overcompaction is thus corrected through modification of the velocity.

TWOPOOL has been extended from a one-material code so that it now treats both fuel and steel. To provide a more realistic description of the hydrodynamic motions associated with single-phase regions than is possible with a homogeneous treatment, a distributed particle-in-cell (DPIC) calculation of liquid fuel and steel mass was provided as a option in TWOPOOL.

Porous medium theory has been applied to the problem of the release of fission gas from fuel pin grain boundaries to cracks in the fuel and also to motion in these cracks. This diffusion could be important in determining pressurization of the clad by fission gas and axial motion of fission gas during a transient. It is estimated from the theory that the time constants for these processes are in the range of tens of milliseconds.

B. Study of Basic Problems in Accident Analysis

1. FX2-POOL/USEFUL Calculations of Fuel-Steel Heat Transfer Effects in HCDA (S. Hakim (RAS Division), R. Henninger (LASL) P. B. Abramson and T. A. Daly)

A $50/sec HCDA run with SAS was converted to FX2-POOL input (except material velocities), a modification was made to FX2-POOL to allow super position of an arbitrary external ramp rate, and a base case was run at 10 ms from the initiation of the prompt burst. From examination of marker particle plots it was decided that approximately 6.2 ms after prompt criticality represented the proper time to make the transition from FX2-POOL to USEFUL. (The USEFUL code, developed by S. Hakim and R. Henninger, calculates the penetration of a hot fuel steel mixture through a pin bundle and includes ablation of cladding and various heat transfer mechanisms). Figure 1 show the marker particle distribution at that time. The scenario being calculated is for a sodium out HCDA and the phenomenon being examined is fuel to steel heat transfer. Results indicate that steel cladding in the upper axial blanket and fission gas plenum could act as a heat sink to reduce the fuel work energy by one to two orders of magnitude. Radial temperature gradients caused earlier axial penetrates by the molten fuel steel mixture of inner channels, with the resulting incoherence causing a further reduction in system damage potential by creating radial incoherence in sodium slug acceleration. This effect has also been observed in a SIMMER calculation.[1]

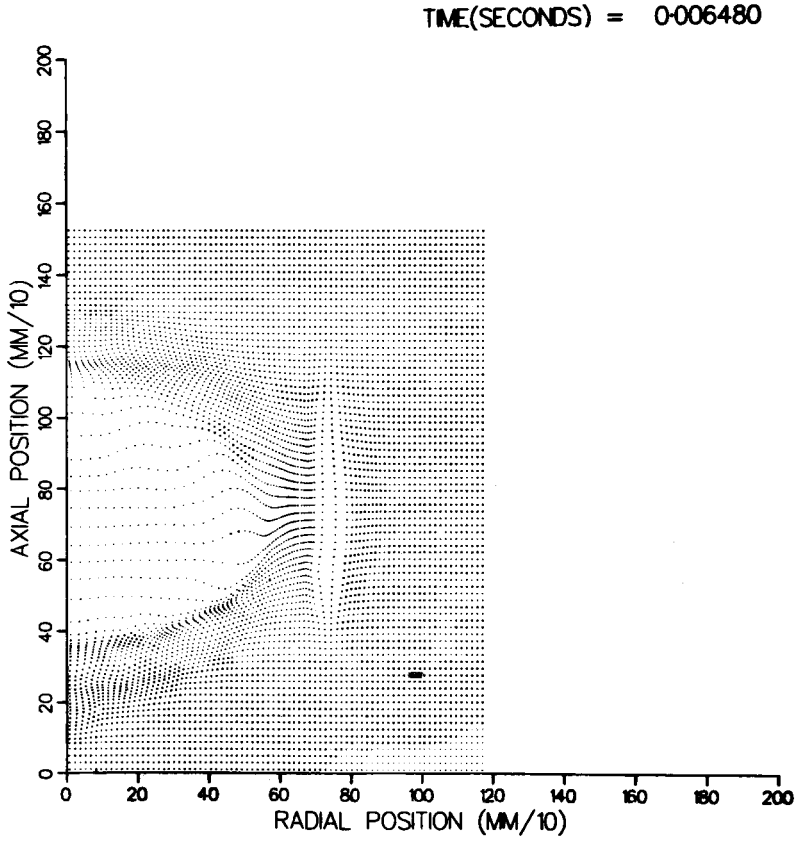

Fig. 1. Particle Distribution From HCDA
ANL Neg. No. 116-77-536

2. Stochastic Mechanistic Analysis of Reactor Transients (P. B. Abramson, H. H. Hummel, E. M. Gelbard, J. J. Sienicki and P. A. Pizzica)

In the use of large computers to analyze severe accidents in LMFBR's it has long been recognized that many of the fundamental phenomena cannot be precisely predicted because of uncertainty in parameters which govern them. As a direct results, analysis of such accidents has proceeded along a parametric path in which these variables were held fixed at a certain constant value for the entire calculation: the influence of variation of this value has been assessed by making a series of complete calculations with the parameter set at a different value for each such element of the series. Recent work by Ott et al[2,3] and Mueller et al[4,5] has described methodology for dealing with uncertainty in parametric value for parameters which do not fluctuate. While some paraters may be thought of as "correlated" or fixed for an entire calculation, very few are in fact constant throughout a reactor and many are completely uncorrelated, either in space or time, during the hypothetical accident. Thus, such analysis would create a set of results which are not indicative or representative of an accident involving fluctating, uncorrelated, or only partially correlated variable parameters. We describe here our recently developed methodology[6] for dealing with various degrees of uncertainty or fluctuation in these parameters. By using two very different deterministic/parametric codes (FX2-POOL[7] and EPIC[8]) we demonstrate that the treatment of some obviously fluctuating parameters, such as droplet/particle size in a Hypothetical Core Disruptive Accident, as random variables with a certain probability distribution during each complete calculation of a series of calculations produces as much as an order of magnitude less uncertainty in the end result than had been obtained assuming perfect correlation.

The example we have chosen to first illustrate the technique is the HCDA in a large LMFBR. The macroscopic physical parameter we use for this example is the total thermodynamic potential energy in the system - a gross system characterisitic that is of major importance in assessing the potential structural damage. The microscopic variable we have chosen to use is the size of the steel particle/droplet used in the calculation. Since the thermodynamic energy is found both in fuel and in steel, and since during an HCDA the energy is generated in the fuel, energy is tranferred from fuel to steel as the system evolves. Figure 2 shows the evolution of the system's available work energy using steel particles whose surface areas are all identical. Three separate systems are represented (dashed lines) and their evolution followed- a system with steel particles of area 1 cm^2, one with 0.1 cm^2 and one with 0.01 cm^2. This is an example of analysis using the fixed parameter approach. We note that the predicted available work energy at 30 ms varies from approximately 10^7 to roughly 2×10^8 Joules i.e. a factor of about 20. Also plotted on Fig. 2 (solid lines) are 4-separate runs treating the particle size as randomly variable during the calculation using a specific probability distribution over the same size range. We note that the results of the 4 different random calculations are nearly repeatable. This is partially due to the fact that a separate parametric value was drawn so many times (for each of 400 cells at each of 50 time steps) but, for the most part the repeatability is due to the fact that we are taking advantage of the distributed (rather than lumped) nature of the parameter. Although the stochastic calculations are somewhat sensitive to cell size and time step size, the prime effect of this technique is to add information that the probability drops to zero near the ends of its band width and that to assign a single constant value near

the end of the band would be to lose that information. Thus the major factor becomes the shape of the distribution function. In Fig. 3 we plot results for several stochastic runs with a broad probability distribution (dashed lines) vs. several runs with a narrow distribution (solid lines) with both distributions falling to zero at the ends of the band used for the calculation in Fig. 2. We note that the spread from one distribution to the other is more than an order of magnitude less than that obtained with the old methodology.

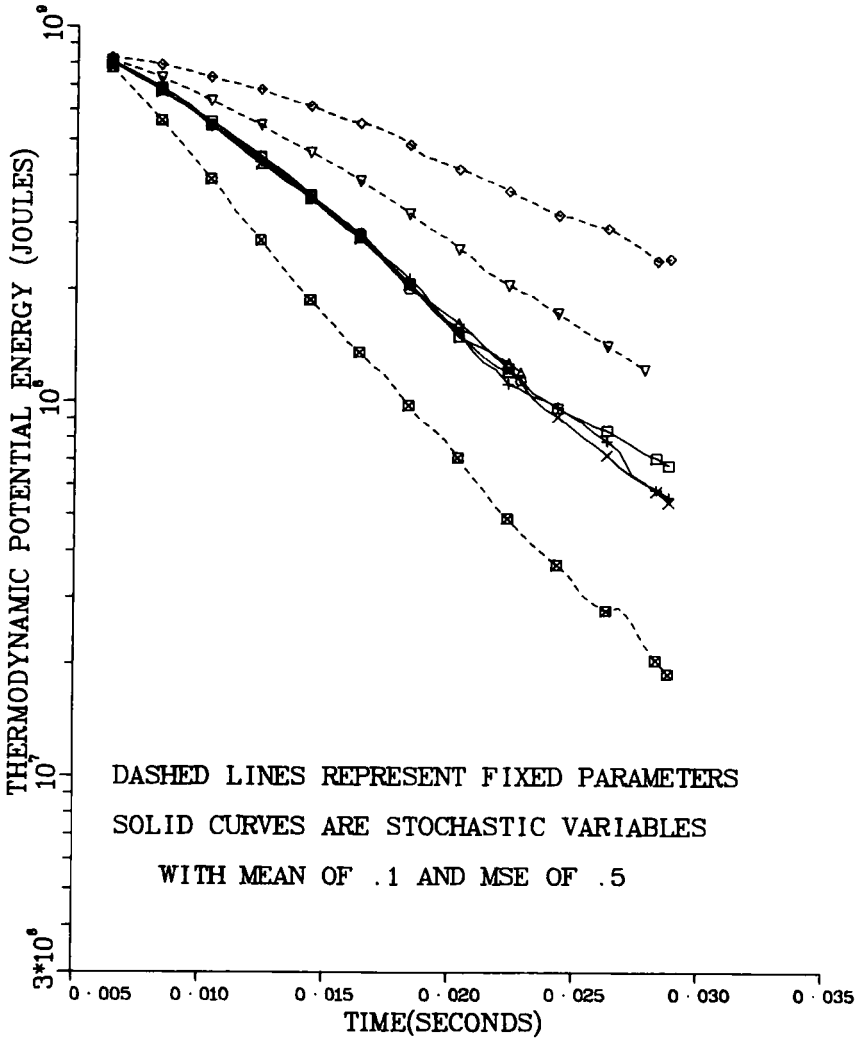

Fig. 2. Stochastic Drop Size Effect on Energy
ANL Neg. No. 116-77-401

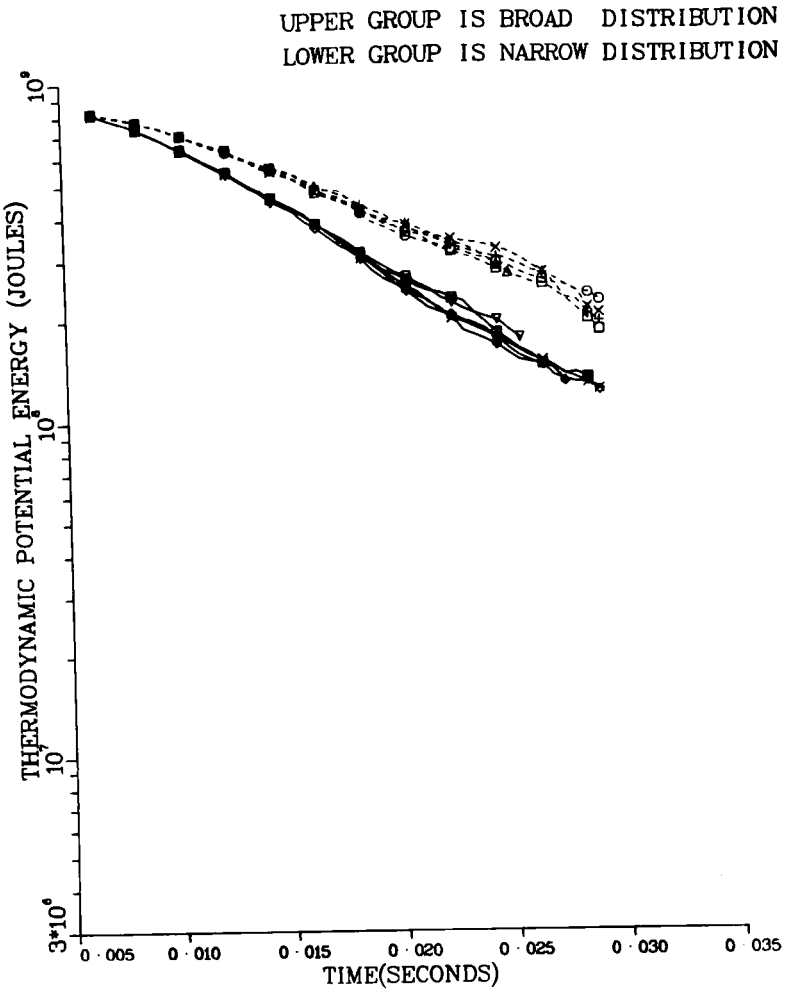

Fig. 3. Probability Distribution Effect
ANL Neg. No. 116-77-460

We have also applied this concept to fuel fragment size in a LOF-TOP calculation with EPIC. Figure 4 shows the sodium reactivity ramp obtained when performing the calculation using different constant values of fragment size (dashed) or using a flat probability stochastic calculation over the same range (solid lines) while Fig. 5 shows the variation of those results using a broad (solid) vs. a narrow (dashed) distribution function.

We conclude that adding to the band width information on parametric values the information that probability must drop to zero at the ends of that band width and adding treatment of those fluctating parameters as such will significantly reduce the calculated uncertainty in macroscopic behavior. Adoption of this philosophy will reduce the task of experimental validation of deterministic codes from the current enormous objective of obtaining the specific single value for each parameter under all possible conditions to one of obtaining only the band width and the bounds on the shape of the distribution function. The technique can be easily implemented (for those truly fluctuating parameters) in a broad spectrum of deterministic codes.

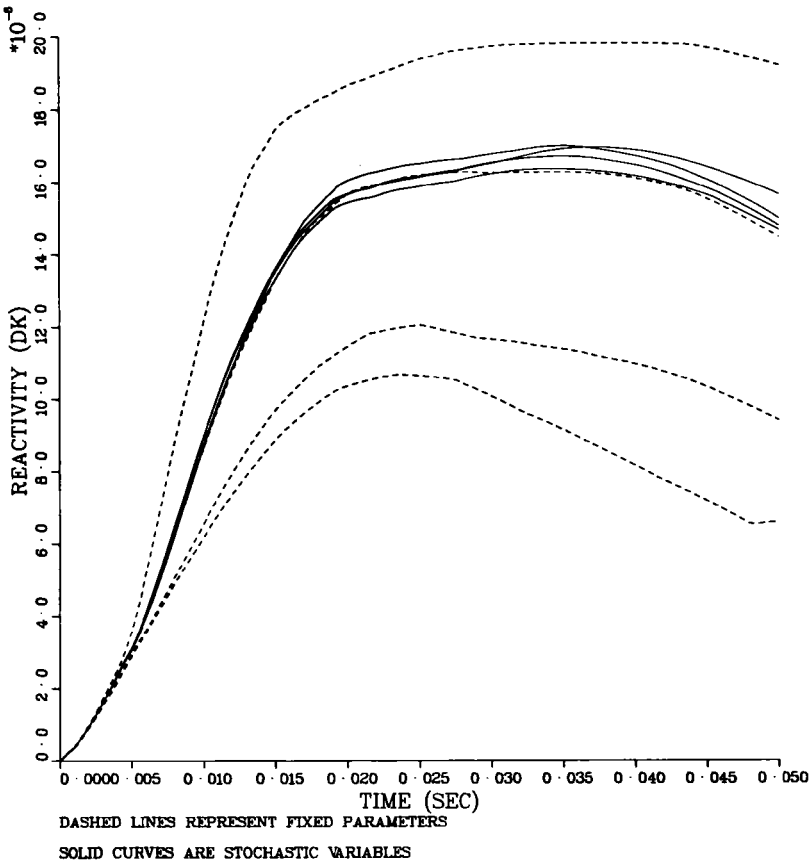

Fig. 4. Stochastic Fragment Size Effect on Sodium Void Reactivity ANL Neg. No. 116-77-400

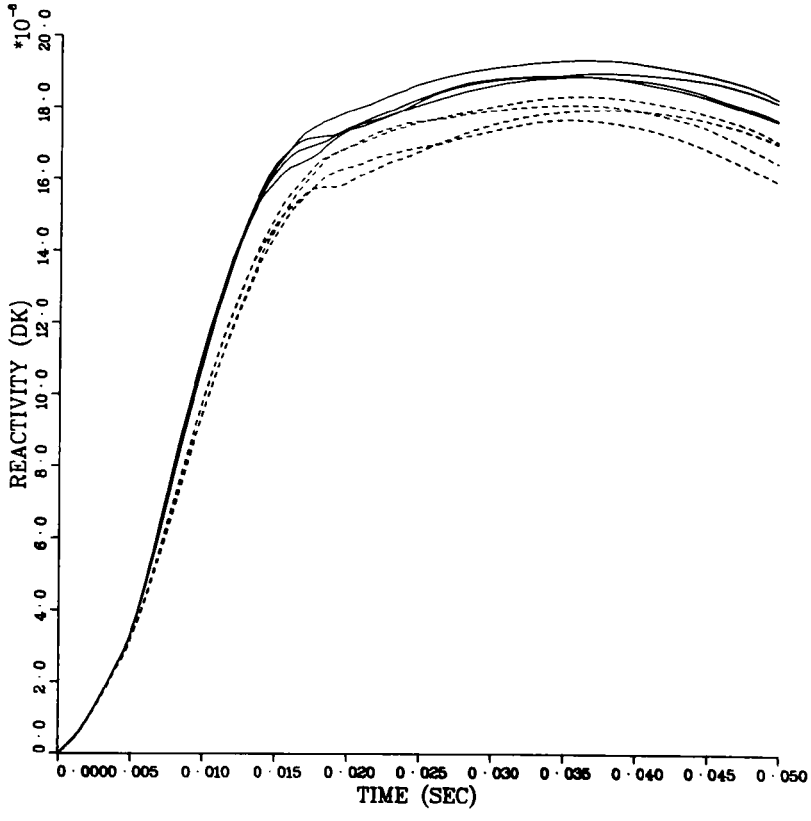

Fig. 5. Sodium Voiding Reactivity Vs. Time ANL Neg. No. 116-77-461

3. Behrens Effect (P. B. Abramson)

Studies of the increased streaming reduction phonomenon by bubble collapse were concentrated upon the effects of local surface compactions. While our studies of local compression without the bubble collapse effect have indicated that rather large surface areas must be pressurized in order to cause significant reactivity increases, our models predict that a full order of magnitude increase in reactivity gain can be obtained by the bubble collapse induced streaming reduction. This effect needs further attention, particularly from a neutronic point of view.

4. EPIC Development (P. A. Pizzica)

An improved fuel vapor ejection model was included in the code as follows: The amount of void in the coolant channel is determined (which includes the void created by the compression of the sodium at the pin ejection node pressure). Enough fuel is then ejected into the coolant channel void to make the fuel smear density in the void equal to the fuel smear density in the pin cavity at the ejection node. Fuel vapor condensation is included in the coolant channel as an energy loss to the two-phase fuel system. The condensation coefficient is a parameter which must be varied within "reasonable" bounds (or otherwise). In the fuel pin cavity, energy is taken out of the two-phase fuel system as the vapor does work on the surroundings by expansion and motion of fuel into the coolant channel, and energy is also taken out of the liquid fuel as more vapor is boiled off to pressurize the void (newly created by the ejected fuel) at the saturation pressure corresponding to the liquid fuel temperature. This energy loss to the liquid fuel in the ejection node in the pin lowers the temperature and thus the pressure causing a (usually slight) pressure differential toward the ejection node if the neighboring nodes were at about the same temperature. The pressure gradients follow the temperature gradients because the saturation curve is always followed and in a fresh pin failure, there is no fission gas partial pressure.

EPIC has been made operational at both SANDIA and HEDL, where the code is being used for fresh pin failure experimental analysis.

The linking of EPIC with SAS3D is continuing but progress has been retarded because of other commitments.

5. EPIC Parameter Studies (P. A. Pizzica & J. J. Sienicki)

The PLUTO-EPIC comparison studies, of which some examples were given in the last quarterly, was completed. The EPIC parameter study was completed as well and a full report is forthcoming.

Selected cases of calculations of the parameter study are presented for 50 ms following pin failure in a demonstration sized reactor using the EPIC computer code. Unless otherwise specified, the initial conditions are 50% midplane melt fraction at pin failure, 3500°K molten fuel average temperature, pin pressure of 190-240 atm, 5 cm midplane failure, and particle radius of 250 microns for fragmented fuel in the coolant channel. The cases described are for TOP conditions and for LOF-TOP conditions.

When four failure locations were compared (15 cm below, at, 15 cm above, and 30 cm above the midplane), approximately the same amount of fuel was ejected in the first three cases but less in the highest failure because the molten fuel fraction there is significantly less and it is more difficult to move fuel up through the smaller orifice in the cavity. This meant a more delayed FCI in the last case and it affected channel pressures and material motions accordingly. Failure location thus caused about an order of magnitude spread in the reactivity insertions (see Fig. 6).

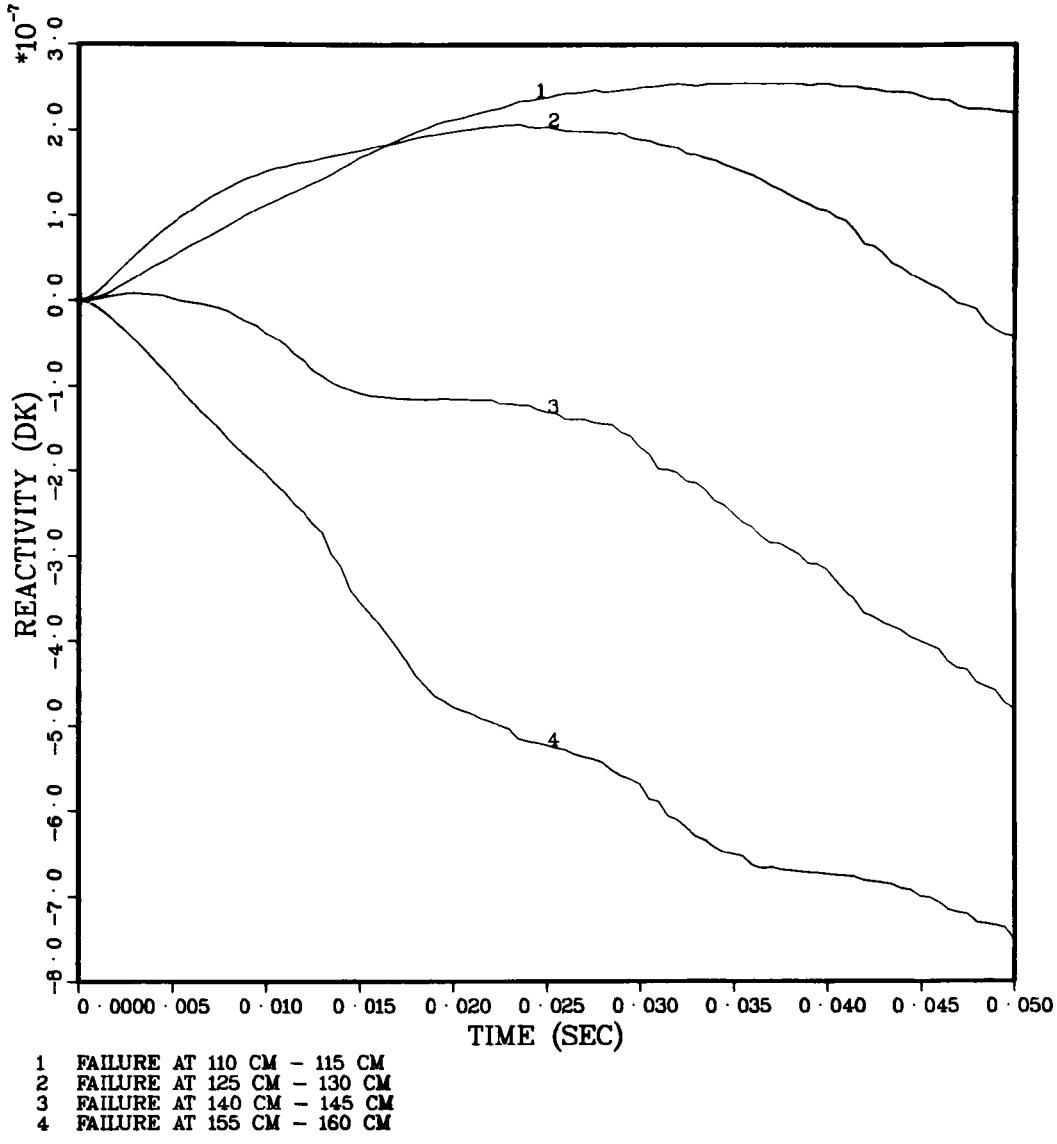

Fig. 6. Total Reactivity for Four Different Failure Locations
ANL Neg. No. 116-77-550

Failure size was varied from a 5 cm rip at the midplane to a 20 cm rip from the midplane up and a 40 cm rip from 10 cm below the midplane to 30 cm above. The last case ejects the most fuel but levels off after ∿15 msec. The second case ejects more than the first initially and then falls behind later on. The first case has the largest and fastest positive reactivity insertion because of the fuel motion in the cavity toward the centerline failure (see Fig. 7). The second case ejects fuel from the upper end of the failure which mitigates this effect. In the last case, so much fuel is ejected high up in the channel that the fuel reactivity goes negative immediately and soon exceeds the magnitude of the positive sodium void.

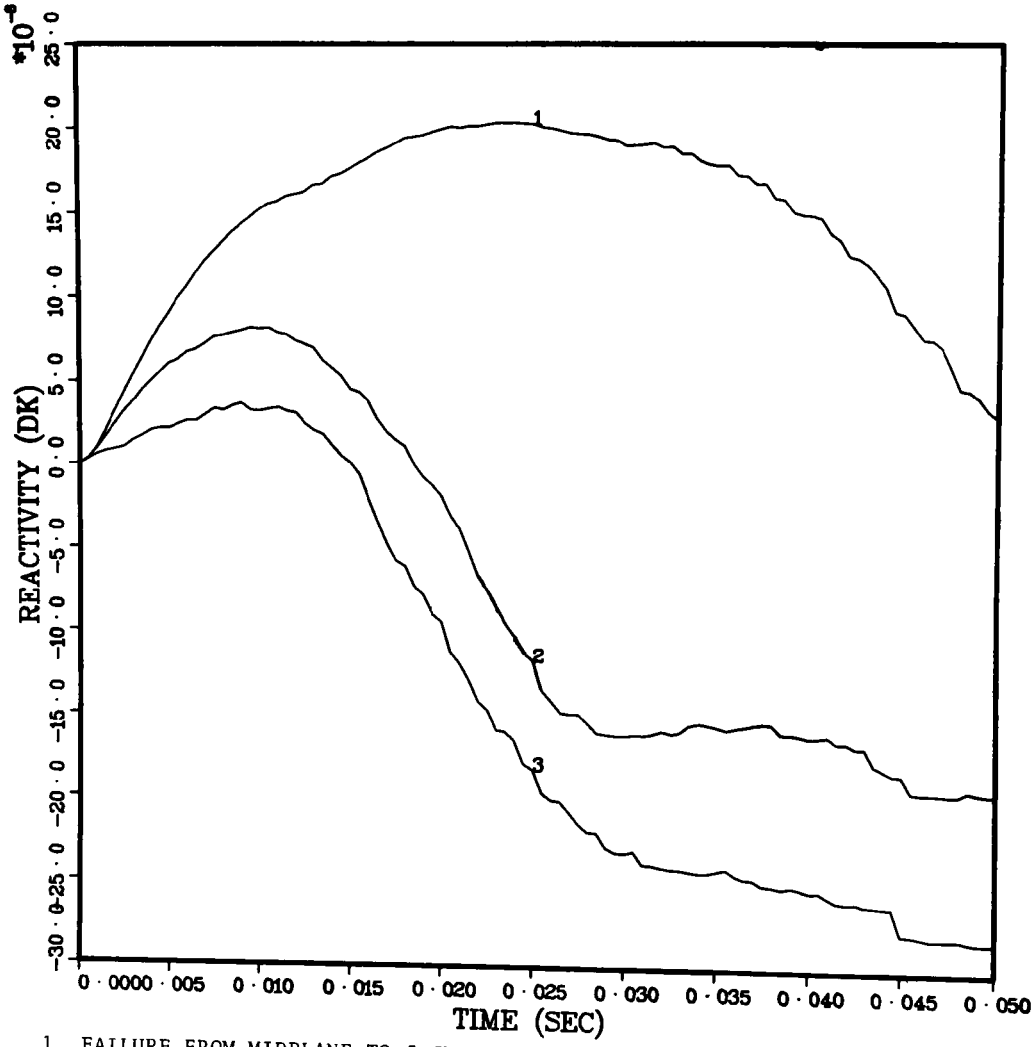

1 FAILURE FROM MIDPLANE TO 5 CM ABOVE MIDPLANE
2 FAILURE FROM MIDPLANE TO 20 CM ABOVE MIDPLANE
3 FAILURE FROM 10 CM BELOW MIDPLANE TO 30 CM ABOVE MIDPLANE

Fig. 7. Total Reactivity for Three Different Failure Sizes
ANL Neg. No. 116-77-549

Two cases were run where fission heating of the fuel and enlargement of the molten fuel cavity from solid-fuel melt-in were varied. The first case corresponded to the power rise associated with an LOF-TOP transient with no autocatalytic power rise and the second to an LOF-TOP with an autocatalytic power rise due to TOP-systle pin failure in lower power subassemblies. The major result is that the amount of fuel ejected is very slightly more in the autocatalytic case util the fuel temperature rises enough ($\sim$15 msec after failure) to cause pressure gradients away from the midplane failure which retards fuel ejection and allows significantly less fuel to be ejected than in the non-autocatalytic case. Fuel reactivities for fuel are therefore higher for the autocatalytic case at first and then begin to fall significantly behind as fuel is moved in the pin away from the midplane.

Cases for three particles radii were run: 100, 250 and 500 microns (see Fig. 8). Very little FCI occurred in the last case - the sodium never exceeded 1200°K (the clad temperature) because of the condensation of sodium vapor on the clad. In the 250 micron case, the sodium reached 1500°K by about 10 msec before the voiding of the channel cut off the heat transfer. With the small 100 microns radiums, an extreme FCI resulted with sodium reaching 2200°K. The FCI in the last case cut off fuel ejection for 7-8 msec but the total mass ejected exceeded the other cases by 50 msec. The 500 micron case ejected more fuel than the 250 micron case because it was swept up the channel faster due to the higher drag. Otherwise, the differences in material motions and reactivities are caused by the difference in the FCI.

When initial fuel temperature was varied (3500, 4000 and 4500°K), the material motion, FCI and reactiviteis varied in an expected fashion (i.e. more fuel ejected with higher temperatures, higher pressures, etc.) according to the fuel temperature including the effect of the significant fuel vapor pressure for the third case.

In the fuel vapor driven ejection case, the results are strongly dependent upon the amount of fuel vapor condensation in the coolant channel. The controlling factor in determining how much fuel is ejected is the difficulty of moving fuel in the pin cavity toward the clad rip when very little pressure gradient exists in the cavity (since the pressure is determined by the saturation pressure of the liquid fuel temperature which is changing little from node to node in the cavity).

When the initial void fraction in the coolant channel was varied between 60, 80 and 95%, the resultant material motions and reactivity changes (see Fig. 9) are a direct result of the severity of the FCI which is more severe for smaller void fractions.

A final case was run for an 80% voided channel with a clad rip which began at 10 cm, expanded to 20 cm at 2 msec after pin failure, to 30 cm at 4 msec and finally to 40 cm at 10 msec after failure. The results did not differ radically from the single node failure for the 80% voided channel, although about 15% more fuel was ejected.

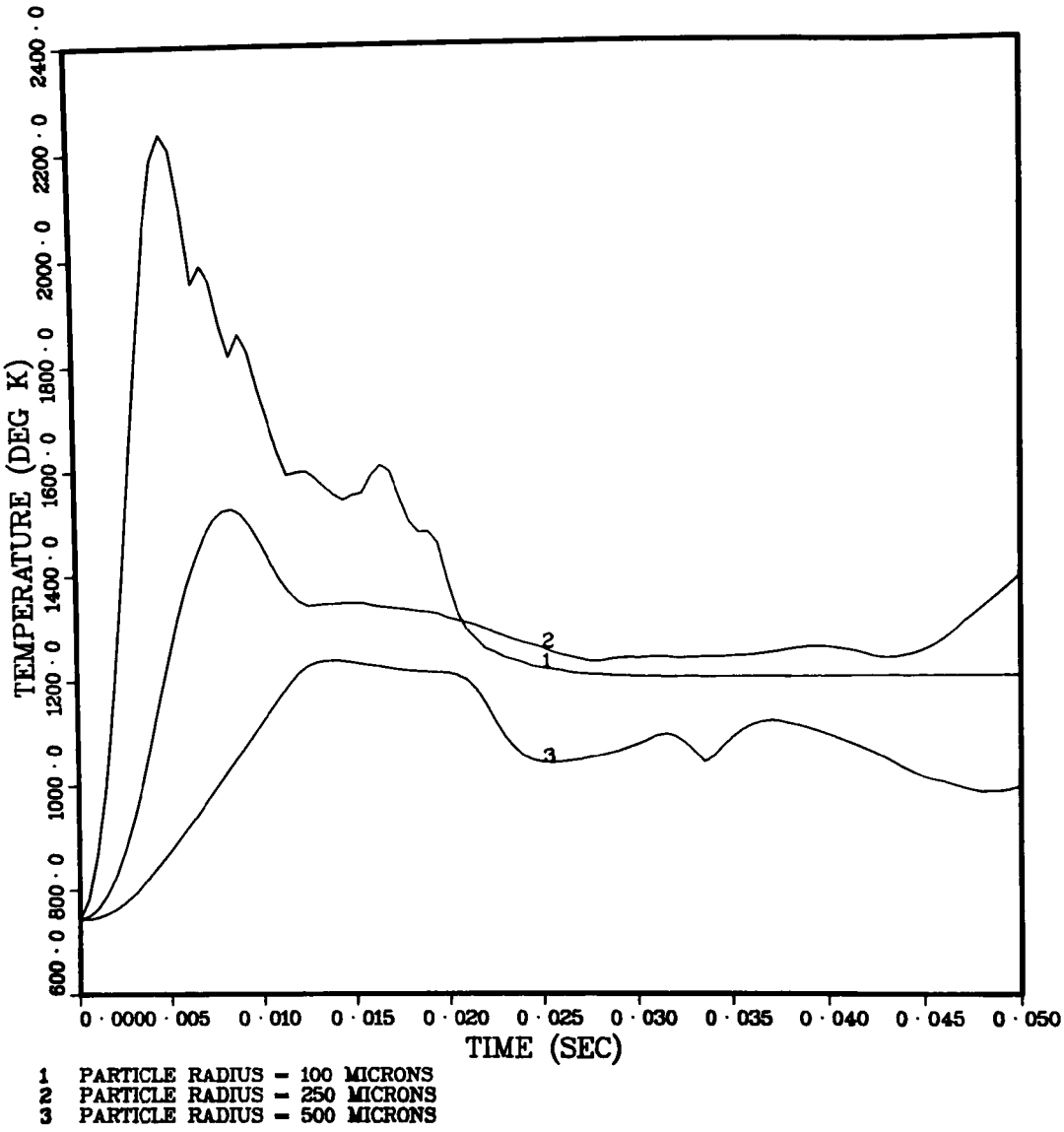

Fig. 8. Sodium Temperature at the Ejection Node for Three Particle Radii ANL Neg. No. 116-77-544

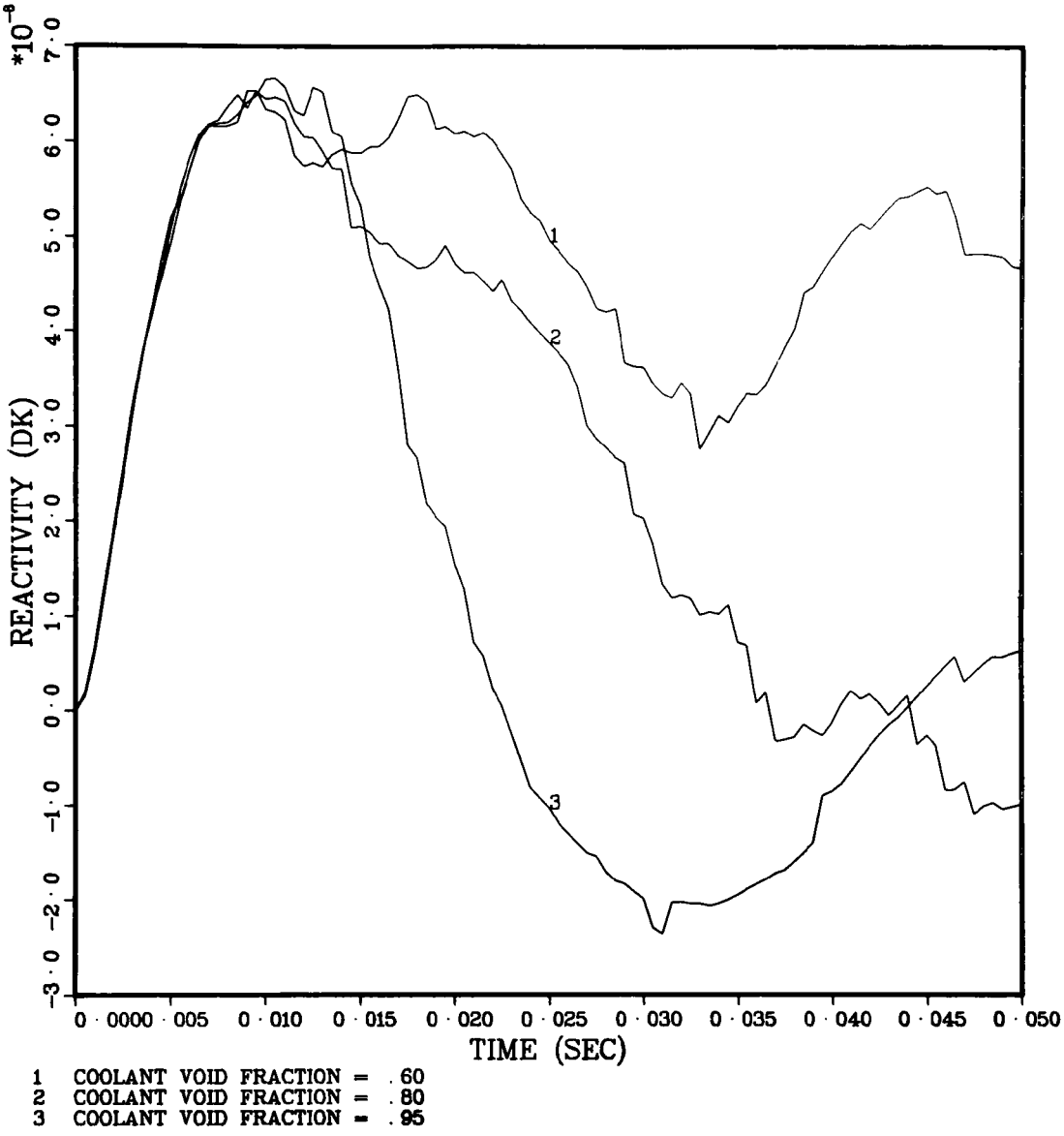

Fig. 9. Total Reactivity for Three Void Fractions
ANL Neg. No. 166-77-538

6. Treatment of Single-Phase Regions in Fast Reactor HCDA's
(J. J. Sienicki & P. B. Abramson)

To follow extended motions in high ramp fast reactor HCDA's, it is necessary to calculate the hydrodynamic motions in single phase regions. A major problem is that the equations which one solves to predict new densities can predict overcompactions of the fluids in computational cells. The approach used in KACHINA and SIMMER for this overcompaction problem is to destroy all excess mass which enters a single phase cell and calculate new velocites assuming that the vapor volume fraction is exactly zero. Such destruction of mass is not a satisfactory solution of the overcompaction problem since it may lead to unrealistic neutronic effects. Furthermore, the velocities thus determined may themselves cause a tendency for continuing overcompaction. Our past approach has centered about uncoupling radial and axial motions in single phase regions. This is an approximation which is valid for only a few cases. We report here on the development of an approach for calculating the hydrodynamic motions in single phase regions which successfully deals with the overcompaction problem for all calculations we have done to date. This approach has been implemented in TWOPOOL and is currently being implemented in POOL.

A computational cell in TWOPOOL is considered to have become single phase when its liquid volume fraction exceeds one. For a single phase cell (centered at i, j), our approach consists of solving the finite difference equations

$$(\bar{\nabla} \cdot \bar{U})^{n+1}_{i,j} = \frac{r_{i+1/2} U^{n+1}_{i+1/2,j} - r_{i-1/2} U^{n+1}_{i-1/2,j}}{r_i \delta_r}$$

$$+ \frac{V^{n+1}_{i,j+1/2} - V^{n+1}_{i,j-1/2}}{\delta z} = \begin{cases} \dfrac{VF^{n+1}_{\ell i,j} - 1}{\delta t}, & \text{if } VF^{n+1}_{\ell i,j} > 1 \\ 0, & \text{if } VF^{n+1}_{\ell i,j} \leq 1 \end{cases} \qquad (1)$$

$$\frac{U^{n+1}_{i+1/2,j} - U^{n}_{i+1/2,j}}{\delta t} + (\bar{U} \cdot \bar{\nabla} U)^{n+1}_{i+1/2j}$$

$$= - \frac{1}{\rho^{n+1}_{i+1/2,j}} \frac{P^{n+1}_{i+1,j} - P^{n+2}_{i,j}}{\delta r}, \qquad (2)$$

$$\frac{V^{n+1}_{i,j+1/2} - V^{n}_{i,j+1/2}}{\delta t} + (\bar{U} \cdot \bar{\nabla} V)^{n+1}_{i,j+1/2}$$

$$= - \frac{1}{\rho^{n+1}_{i,j+1/2}} \frac{P^{n+1}_{i,j+1} - P^{n+1}_{i,j}}{\delta z} \qquad (3)$$

where $\bar{U}$ is the liquid velocity with radial component U and axial component V, VF_ℓ is the liquid volume fraction, P is the pressure, and ρ is the liquid "physical density" (liquid smeared density divided by the liquid volume fraction). δt is the time step from cycle n to cycle n+1. r is the radial coordinate. δr and δz are the radial and axial mesh cell widths.

In Eq. (1), $(\bar{\nabla} \cdot \bar{U})^{n+1}_{i,j}$ is the rate of increase of liquid volume fraction of the cell. $VF^{n+1}_{\ell i,j}$ is the relative volume which the single phase material would occupy if velocities were not corrected during the time step. According to Eq. (1), end of time step velocities are chosen to move excess liquid out of the cell such that it fills the correct volume at the end of the time step. Overcompactions are thus corrected through modifications of the velocities.

To solve Eqs. (1) - (3), $U^{n+1}_{i+1/2,j}$, $U^{n+1}_{i1/2,j}$, $V^{n+1}_{i,j+1/2}$, $V^{n+1}_{i,j1/2}$ obtained from Eqs. (2) and (3) at the four cell edges are substituted into Eq. (1) to obtain a Poisson equation for the single phase pressures. This pressure equation is solved for all single phase cells during each semi-implicit interation step using an ANL elimination routine (CROUT).[9] A direct solution using an elimination process is computationally viable because the number of single phase cells is typically only a fraction of the total number of mesh cells in the HCDA problems which we are considering. A reason for choosing an elimination process over iterative methods such as the iterative pressure formulation ICE techniques is the large magnitudes and spatial variations characteristic of single phase pressures (typically serveral orders of magnitude greater than two phase pressures) which might hamper the convergence of an iterative solution.

The TWOPOOL approach has been observed to result in liquid volume fractions in single phase cells which remain close to one (typically within a few tenths of a percent) and allow hydrodynamic motions to be followed well after single phase material splashes off of the computational boundaries.

We have also observed that the liquid volume fraction of some cells which were incompressible decreases below one on a given cycle (and is thus treated as two phase) and may later become single phase again. Such swings in the single phase/two phase character can be stabilized by defining a threshold such that VF_ℓ must decrease below this threshold before a single phase cell is again considered two phase. Such a threshold is presently an input parameter in TWOPOOL.

7. Extension of TWOPOOL to Two Materials (J. J. Sienicki)

TWOPOOL was extended from a one material code to one which treats both fuel and steel. Liquid fuel and steel are assumed to move together with a common liquid velocity as are their vapors. As in POOL, liquid fuel is assumed to remain in thermal equilibrium with fuel vapor while liquid steel is assumed to separately remain in thermal equilibrium with its vapor. The pressure which drives the hydrodynamic motions in two phase regions is taken to be the sum of the fuel and steel vapor pressures.

Heat transfer between liquid fuel and liquid steel is modeled as the sum of a convective term and a radiative term which depend parametrically upon a heat tranfer coefficient, the droplet radius, and a fraction of the steel droplet area exposed to liquid fuel. This heat transfer between fuel and steel is formulated in a linearized fully implicit fashion to allow the treatment of arbitrarily high heat transfer rates.

In addition to fuel to steel heat transfer, the partially implicitly coupled TWOPOOL equations for the fuel and steel temperatures and the liquid fuel, liquid steel, and vapor volume fractions include for each material effects of the assumed rapid liquid-vapor heat transfer which maintains the thermal equilibria, vaporization and condensation, convection of liquid and vapor mass and energy, fission heating of liquid and vapor, and compressional work performed on each vapor. For each material the vapor pressure, heat of vaporization per unit mass, liquid and vapor physical densities, liquid specific heat per unit mass, and liquid internal energy per unit mass are general temperature dependent functions. Appropriate thermophysical properties have been included for both liquid and solid temperature regimes.[10] The melting/freezing phase transition for each material is treated by assuming that the phase transition occurs continuously over a finite (small) temperature range, thus eliminating the need for keeping track of the fraction of heat of fusion satisfied.

8. Inclusion of DPIC in TWOPOOL (J. J. Sienicki)

To provide a more realistic description of the hydrodynamic motions associated with single phase regions than is possible with a purely homogeneous treatment, a distributed particle-in-cell (DPIC)[11] calculation of liquid fuel and liquid steel mass convection was added to TWOPOOL. Choice of using DPIC or the older homogeneous treatment is provided as a user determined option. We plan to study the relative effectiveness of different particular implementations of DPIC in a two field, two phase code such as TWOPOOL.

J. J. Sienicki attended the five day Liquid Metal Fast Breeder Reactor Safety Technology Study at Northwestern University, May 2 - 6, 1977.

9. Motion of Fission Gas Released from Grain Boundaries of a Fuel Pellet (Kalimullah)

The axial motion of fission gas released into fuel pellet cracks is important in clad failure analysis because it is the gas in the cracks (and not at grain boundaries) which exerts primary pressure on the cald. Axial motion determines the distribution of the gas along the length of the pin and the amount going into the plenum. Assuming that there is no axial motion of

the gas released into the cracks will give the highest pressure. This pressure for a CRBR fuel pin at 100,000 MWD/MT burnup, assuming (1) a gas temperature of 2500°K (2) a pore-plus-gap (cold dimensions) volume of 15% (3) retention of about 20% of the produced fission gas in the steady state (4) release of about 30% of the retained gas during the transient and (5) about 50% unrestructured fuel, is about 43 atmospheres, resulting in a clad hoop stress of about 4200 psi. Expansion of the fuel during the transient will decrease the gas volume and correspondingly increase the pressure.

The axial motion of the fission gas may be analysed by treating the column of cracked pellet pieces as a porous medium. A fuel column of cracked pellets has two types of porosity and particle size associated with its complete analysis. The cracked pieces are one type of particles and the gap between them is the porosity for gas flow even if the particles themselves were not internally porous. Since the pellets are never of their theoretical density, the cracked pieces have internal porosity and this is the second type of porosity associated with the fuel column. The particle size associated with the second type of porosity is usually very small (a few tens of microns) compared to the cracked pieces, and these particles may be the grains themselves. As far as axial gas flow to the plenum is concerned, almost all of the flow will occur through the external porosity, i.e., the gaps between the cracked pellet pieces (because the permeability of the internal porosity is a few orders of magnitude smaller than that of the external porosity, permeability being proportion to the square of particle diameter) and the contribution of the internal porosity will be negligibly small.

A brief summary of equations for flow in a porous medium and their experimental validy is given below. Overall the status of porous medium analysis is quite satisfactory and the theory compares very well with the experimental measurements.

Viscous flow through a porous medium:

Since the flow through a porous medium is of a creeping nature (low speed) and the hydraulic diameters of the flow passages are quite small, the flow is invariably viscous due to low Reynolds numbers involved. Based on the semi-theoretical works of Blake and of Kozeny and Carman summarised in reference 12, the apparent linear velocity of flow, U is related to the pressure gradient in the direction of flow by the equation

$$U = - \frac{\varepsilon^3}{k_o q^2 S^2} \frac{1}{\mu} \frac{\partial p}{\partial x} = - \frac{B_o}{\mu} \frac{\partial p}{\partial x} , \qquad (4)$$

where $\frac{\partial p}{\partial x}$ = pressure gradient of the fluid in the pores in the direction of flow,

ε = pore volume per unit volume of the porous medium called porosity,

S = surface area of the particles per unit volume of the medium called the specific surface area of the medium,

μ = viscosity of the fluid,

q = average length of the fluid flow path through the medium divided by the length of the test-piece called tortuosity,

k_o = a dimensionless constant, experimentally determined to be about 2.5, and

B_o = the quantity in the parentheses called permeability.

This equation has been verified experimentally by a number of workers[12] for large number of (a) porous beds (including beds made of alundum, black slate powder, carborundum powder, celanese yarn, copper wires, fiber glass, glass fibers, glass powder, glass sand, glass wool, kaolin, kiesel guhr, mica, nickel rings, porcelain pieces, pyrex, quartz sand, sand, sandstone, silica powder, sintered glass, steel wire crimps, steel wool), (b) particle shapes (including spheres, cylinders, hexagonal prisms, cubes, square plates, triangular prisms, discs), (c) particle sizes from 2 microns to about 1/4 inch and (d) porosity from 0.14 to 0.89. The value of the constant k_o is found to be in the range 2.5 ± 0.5.

The value of the tortuosity q in Eq. (4) depends upon whether the porous medium is unconsolidated (i.e., made up of discrete particles by allowing them to settle into contact under gravity by tapping the container) or consolidated in which the solid part forms a continuous and permanent structure. (In many cases consolidated porous media are formed from particles which are not merely in contact but have been welded together by sintering processes, by substances deposited from solution, etc.) A UO_2 pellet is a consolidated porous body but a column of cracked pellet pieces will behave as an unconsolidated porous medium for gas flow through the cracks. For all unconsolidated porous media $q = \sqrt{2}$ should be used in Eq. (4). Minor variations from this value of tortuosity have already been absorbed in the value of the constant k_o. This value of tortuosity for an unconsolidated medium has the obvious theoretical interpretation of the ratio of the sum of the lengths of two sides of a square to the length of a diagonal.

The value of the tortuosity q for a consolidated medium for use in Eq. (4) should be measured experimentally by measuring the apparent specific electric conductivity of the medium with the pore space filled with an electrically conducting liquid such as a salt solution. Assuming the solid porous medium itself to be a non-conductor, the ratio J of the apparent specific conductivity of the liquid-filled medium to the specific conductivity of the liquid is related to tortuosity by the equation,

$$J = \frac{\varepsilon}{q} . \qquad (5)$$

If the size and shape of the particles are known, the specifc surface area of the medium S may be obtained from the specific surface area of the particles S_o, i.e. surface area per unit particle volume, by using the relation,

$$S = S_o(1-\varepsilon). \tag{6}$$

Equation (4) itself can also be used to evaluate the specific surface area of the medium.

In a simplified model, the release of fission gas from inside the fuel grains to the gas plenum can be thought to involve the following three processes:

(A) Release from the inside of grains to grain boundaries. This process can be analysed with the help of the Gruber's transient gas release model.[13]

(B) Release from the grain boundaries to the gaps between the cracked pellet pieces (the external porosity). This process can be analysed using the Blake-Kozeny-Carman permeability equation, Eq. (4).

(C) Axial motion of the fission gas along the fuel column through the gaps between the cracked pellet pieces. The permeability Eq. (4) can be used to treat this flow also.

Estimate of the time constants for processes (B) and (C):

The continuity equation in one-dimension for flow in a porous medium can be written as[12]

$$\frac{\partial \rho}{\partial t} = \frac{1}{\varepsilon}\frac{\partial}{\partial x}\left[\frac{B_o}{\mu}\rho\frac{\partial p}{\partial x}\right], \tag{7}$$

where ρ is the density of the fluid and t is time. Assuming that the fission gas obeys the perfect gas equation of state, Eq. (7) can be reduced to the following form for isothermal flow:

$$\frac{\partial p}{\partial t} = \frac{B_o}{\varepsilon\mu}\frac{\partial}{\partial x}\left[p\frac{\partial p}{\partial x}\right]. \tag{8}$$

Equation (8) has been put in a non-dimensional form and numerically solved[14] for a tube filled with a porous medium, one end closed and the other open, and the pores of the medium pressurized initially to a uniform high pressure P_1. The transient is started by a step-reduction in the pressure at the open end to P_0 which is kept constant throughout the transient. From the solution, Fig. 8 of reference 14, the time required for the release of about 63% of the mass of gas initially present in the medium is found to be

$$t_r = \frac{\varepsilon\mu L^2}{B_o(P_1-P_0)}, \tag{9}$$

where L is the length of the tube. For reasonable values of the parameters involved in Eq. (9), the residence time t_r is found to be a few tens of milliseconds.

C. Coordination of RSR Fast Reactor Safety Research

P. B. Abramson visited Sandia Laboratory on May 23rd for discussion of SIMMER development experiments with R. Coats, instrumentation development for such experiments with J. Powell, and Corium/concrete interactions with Dirk Dahlgren.

Peter Royl (GfK, Karlsruhe) was at ANL during June and brought some recent POOL calculations from GfK. A bug in the code was diagnosed and a cure (developed here in January 1977) was suggested to him. Recent versions of POOL and the work energy routines were copied for him to take back to GfK.

PUBLICATIONS

The PLOOP Code for the Primary Loop Coolant Flow and Heat Transfer Analysis of Certain Pool-Type LMFBR's
Kalimullah
Proc. Am. Nucl. Soc., November-December 1977, San Francisco, CA.

The Numerical and Modeling Techniques Used in the EPIC Computer Code
P. A. Pizzica and P. B. Abramson
Proc. Meeting on Improved Methods for Analysis of Nuclear Systems, March 1977, Tucson, Arizona.

Comparison of the EPIC and PLUTO Computer Codes for TOP Conditions
P. A. Pizzica, J. J. Sienicki, P. B. Abramson and H. U. Wider
Proc. Am. Nucl. Soc., June 1977, New York, NY.

II. MONTE CARLO ANALYSIS AND CRITICALS PROGRAM PLANNING FOR SAFETY-RELATED CRITICALS (A2018)

A. Monte Carlo Analysis of Safety-Related Criticals (E. M. Gelbard)

Monte Carlo, Transport and Diffusion Calculation for R-Z models of the reference and damaged cores have been complete. The resulting eigenvalues are given in Table I.

TABLE I. Transport and Diffusion Theory Eigenvalues for Step 1 and Step 5 R-Z Models

	DIF (P_1)	TWOTRAN (S_4-P_1)	VIM
REFERENCE CORE	0.9993	1.0093	1.0045 ± 0.0011
STEP 5 DAMAGED CORE	0.9985	1.0133	1.0105 ± 0.0016

Eigenvalue changes from Step 1 to Step 5 are:

$$k^{\text{Step 5}}_{\text{Diff.}} - k^{\text{Step 1}}_{\text{Diff.}} \equiv \Delta_{\text{Diff.}} = -0.0008,$$

$$\Delta_{\text{TWOTRAN}} = 0.004,$$

$$\Delta_{\text{VIM}} = 0.006.$$

The VIM-TWOTRAN eigenvalue differences are about 4σ in the reference core and 2σ in the damaged core.

Comparison of fission source shapes from Diffusion Theory and TWOTRAN calculations for the reference and damaged cores are given in Tables II-V. Analysis of these distributions does not indicate any substantal differences in the two methods of calculation.

B. Planning of Demo Safety Related Experiments (S. K. Bhattacharyya and L. LeSage)

In preparation for the experiments, a safety analysis for the Safety Related Critical Experiments was performed. The analysis consisted of computing the consequences of a Maximum Credible Accident (MCA) and a Design Basis Accident (DBA) for these critical configurations. Of the several planned experimental configurations, it was determined that the fuel slump-out configuration would have the severest consequences. The MCA and DBA analyses were therefore performed for this configuration. Detailed discussions on

TABLE II. Reference Core Fission Source Distribution R = 1.185 cm

Z (cm)	TWOTRAN	DIF THEORY
0.89	0.596-5	0.576-5
4.44	0.592-5	0.573-5
7.99	0.584-5	0.564-5
11.54	0.571-5	0.552-5
15.10	0.553-5	0.535-5
18.65	0.531-5	0.513-5
22.20	0.505-5	0.488-5
26.94	0.464-5	0.448-5
32.07	0.413-5	0.398-5
37.20	0.357-5	0.343-5
42.33	0.298-5	0.285-5
47.59	0.194-6	0.194-6
53.22	0.109-6	0.115-6
58.86	0.670-7	0.688-7
64.05	0.442-7	0.434-7
67.90	0.326-7	0.306-7
71.75	0.239-7	0.212-7
75.59	0.171-7	0.141-7
79.44	0.118-7	0.837-8
83.29	0.728-8	0.345-8

TABLE III. Reference Core Fission Source Distribution Z = 0.89 cm

R (cm)	TWOTRAN	DIF THEORY
1.185	0.596-5	0.576-5
5.925	0.587-5	0.569-5
10.665	0.570-5	0.552-5
15.404	0.543-5	0.526-5
19.760	0.512-5	0.496-5
22.962	0.484-5	0.469-5
26.164	0.454-5	0.439-5
29.366	0.421-5	0.407-5
32.568	0.386-5	0.373-5
35.770	0.349-5	0.337-5
38.972	0.312-5	0.300-5
42.174	0.274-5	0.264-5
45.376	0.238-5	0.231-5
50.176	0.123-6	0.132-6
55.510	0.739-7	0.794-7
60.843	0.468-7	0.484-7
66.176	0.301-7	0.296-7
71.510	0.191-7	0.177-7
76.843	0.118-7	0.971-8
82.176	0.641-8	0.377-8

TABLE IV. Damaged Core Fission Source Distribution R = 0.974 cm

Z (cm)	TWOTRAN	DIF THEORY
0.89	0.212.4	0.199-4
4.44	0.209-4	0.196-4
7.99	0.201-5	0.189-4
11.54	0.188-4	0.177-4
15.10	0.171-4	0.160-4
18.65	0.150-4	0.139-4
22.20	0.121-4	0.114-4
26.94	0.457-6	0.479-6
32.07	0.320-6	0.338-6
37.20	0.239-6	0.244-6
42.33	0.172-6	0.176-6
47.59	0.122-6	0.122-6
53.22	0.800-7	0.783-7
56.86	0.486-7	0.453-7

TABLE V. Damaged Core Fission Source Distribution Z = 0.89 cm

R (cm)	TWOTRAN	DIF THEORY
0.974	0.212-4	0.199-4
4.870	0.206-4	0.194-4
8.776	0.193-4	0.182-4
12.662	0.173-4	0.164-4
16.303	0.752-5	0.719-5
19.117	0.683-5	0.659-5
22.051	0.623-5	0.603-5
24.925	0.566-5	0.548-5
27.799	0.511-5	0.495-5
30.672	0.549-5	0.444-5
33.546	0.408-5	0.394-5
36.420	0.359-5	0.347-5
39.294	0.313-5	0.305-5
44.629	0.151-6	0.164-6
50.784	0.846-7	0.906-7
56.939	0.501-7	0.515-7
63.095	0.303-7	0.298-7
60.250	0.183-7	0.171-7
75.405	0.106-7	0.909-8
81.560	0.544-8	0.342-8

these hypothetical accidents are provided in the Final Safety Analysis Report (FSAR) document for ZPR-6 and -9.[15] Briefly, the MCA is a test of fuel clad integrity under hypothetical accident conditions with trips set two decades too high, and the DBA is a test of cell integrity under accident conditions and with no trips operative.

Figure 10 shows in summary form, the results of the MCA calculation. The reactivity addition causes the neutron density to increase very rapidly as prompt critical is reached. The Doppler effect turns the excursion around and the triggering of the ^{10}B and fuel-bearing safety rods shuts off further reaction. The maximum fuel temperature attained was computed to be 153°C which is well below the FSAR limit of 200°C. Since the calculation used very conservative neutronics parameters and neglected the effects of expansion, the computed temperature-rise is conservative.

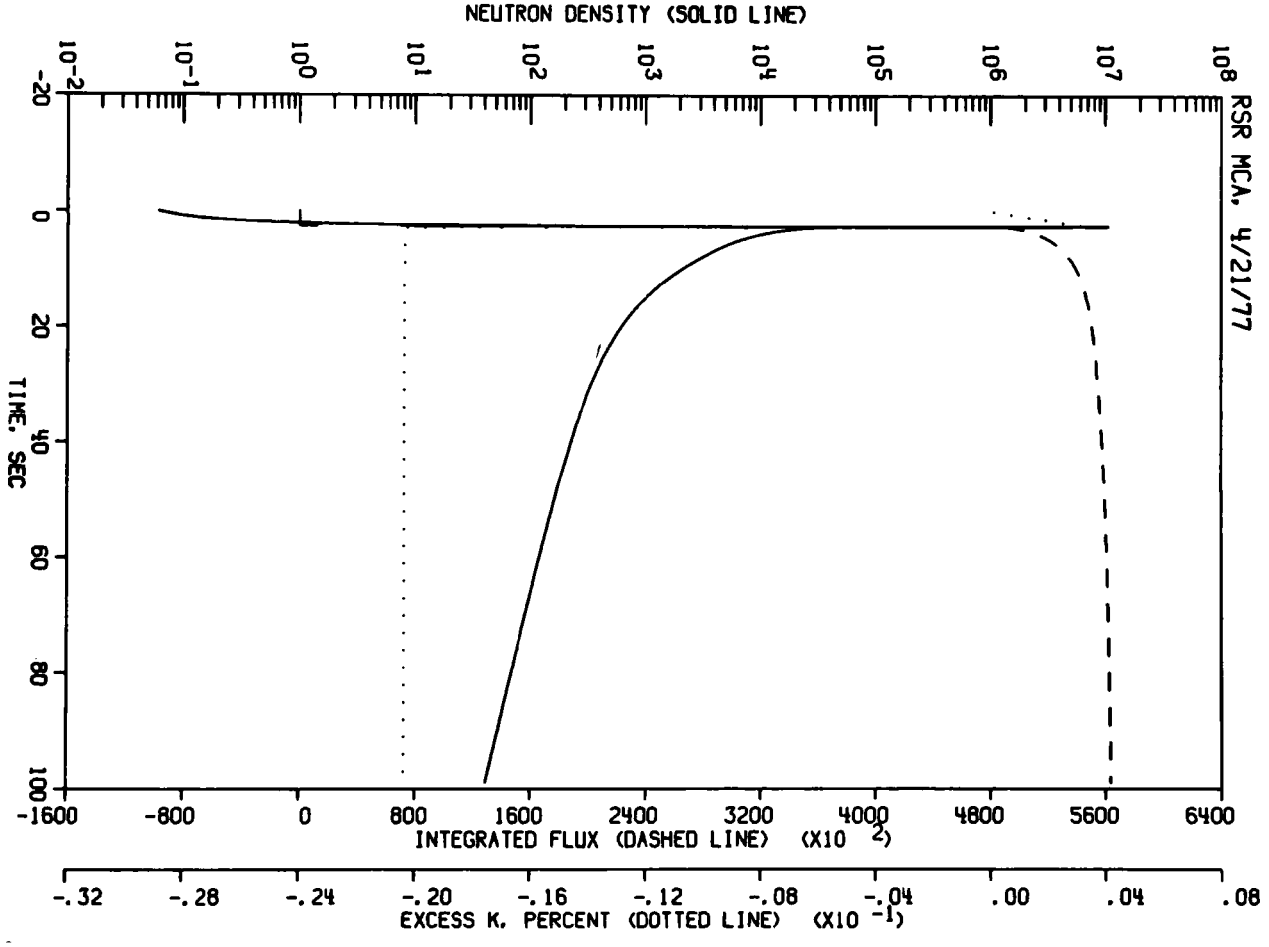

Fig. 10. Summary of the Results of the MCA Calculations ANL Neg. No. 116-77-539

Figure 11 shows, in summary form, the results of the DBA calculation. The accidental addition of reactivity causes a rapid rise in the neutron density as prompt critical is reached. The Doppler and expansion of feedback terms turn the excursion around and a first peak in the neutron density occurs at about 4 seconds. The neutron density then begins increasing again, at a lower rate, until the temperature in the compacted fuel zone exceeds the melting point of fuel (1230°K) and cladding (1670°K) causing molten fuel to start

flowing out of the zone at 15.61 sec. This causes a rapid loss of reactivity from the system and by 15.83 sec the assembly becomes subcritical. By 18.9 sec the assembly is 2.8% subcritical, and the neutron density has dropped to 1% of the peak value and the excursion is over for all practical purposes. At the conclusion of the accident, the pressure in the cell was only 14.7 psia and the total number of fissions during the accident was 1.14×10^{19}. Both these terms are well within the limits imposed by the FSAR. Table VI gives a summary of the analysis results and compares them to corresponding results in the FSAR.

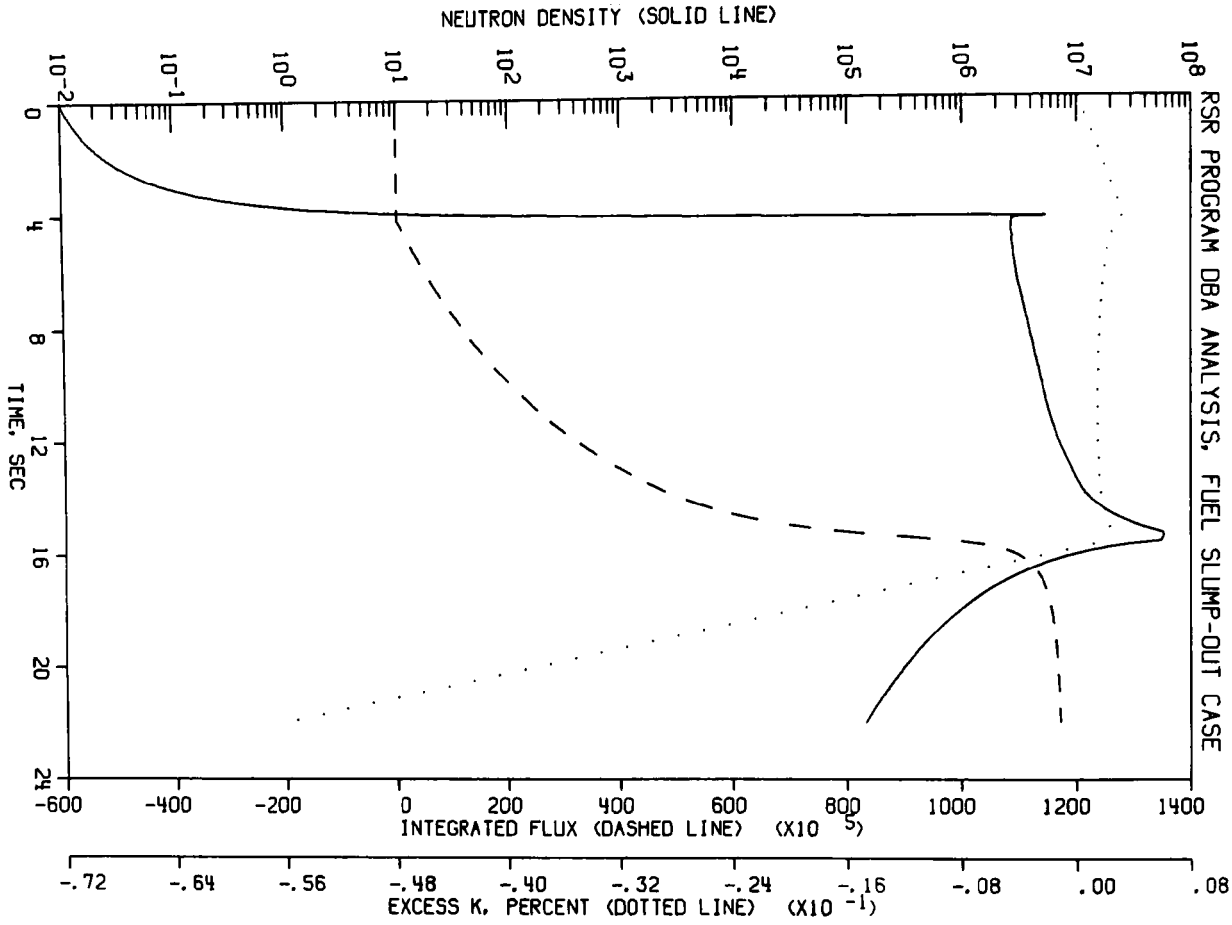

Fig. 11. Summary of the Results of the DBA Calculations
ANL Neg. No. 116-77-540

The results of the analysis showed that the safety parameters for the configurations for the Safety Related Critical Experiments are scoped by the parameters in the ZPR-9 FSAR. It was concluded that the proposed experiments can be carried out safely without undue risk to the health and welfare of Laboratory personnel and to the general public. The Reactor Safety Review Committee of ANL agreed with this conclusion and gave safety approval for the experiment in June 1977.

TABLE VI. Comparison of Safety Parameters of the Demo Safety Related Critical Experiment Cores and the FSAR Reference Core

	Parameter	Safety Core	FSAR Reference Core
1.	Maximum Temperature Increase in fuel as a consequence of a Maximum Credible Accident (°C)	153	200
2.	Maximum fuel temperature in core during a Design Basis Accident (°K).	1870	1850
3.	Total number of fissions in the core in the course of a DBA.	1.14×10^{19}	2.7×10^{20}
4.	Pressure in reactor cell at the end of the transient during a DBA (psia).	14.7	22.6
5.	Weight of sodium boiled (Kg) at the end of transient.	0	9.0
6.	Weight of sodium boiled in total (including final heat balance) (Kg).	0	21.9
7.	Pressure in reactor cell after heat balance (psia).	14.7	34.6 psia
8.	Total Pu inventory (Kg).	410	1354
9.	Quantity of Fuel Melted* (Kg).	60	60
10.	Radioactivity Release.	Smaller	-

*Assumed.

The program plan for the Safety Related Critical Experiments was finalized. Since the time for the program was decreased from 12-15 months to 6 months, some of the phases of the program planned earlier had to be eliminated. The final abbreviated program plan has very little allowance for contingency. Some of the measurements in the program plan have been assigned a lower priority and will have to be eliminated if time pressures so dictate. However, the program as presently detailed, includes the minimum measurements necessary for the validation of analytical methods. The suggestions of the Fast Reactor Critical Experiment Review Group[16] have been incorporated in the planning of the experiments.

The experimental programs that will be undertaken in the various configurations are outlined in Table VII. Some operational measurements (viz operational control rod worths, temperature coefficients, etc) will be performed in addition to those listed for each critical configuration. A depleted uranium reflector will be used to isolate the cores from the reflection effects of the ZPR-9 support structures. The reflector will be composed of depleted uranium blocks loaded in the matrix in stainless steel trays. The reflector will be kept in place for all phases of the program including the blanket collapse phase (Phase V). Because of calculational convenience, the reflector will not be collapsed during the blanket collapse phase of the program. The high degree of compaction in the proposed experiment plan has been questioned and it has been suggested that lesser degrees of compaction might be more prototypical. However, as of this writing, results of SIMMER calculations that might have provided information for a quantitative evaluation of prototypical degrees of compaction, were not available.[17] Since prototypicality was not a necessary requirement for the program, the dense compaction models originally proposed have been retained in the program.

TABLE VII. Program of Measurements in the Safety Related Critical Experiments

Phase/Step (See Table I)	K_{eff}	Neutron Spectrum	Central Reactivity Worth	Axial Worth Profiles	Reaction Rate Profiles[a]	Doppler Worth of ^{238}U	Central Control Rod Worth	Prompt Neutron Lifetime	Beta Effective
1. 1 A (Reference Core)	✓	Core Center	^{239}Pu, ^{240}Pu, ^{238}U U, B, Na Stainless Steel	^{239}Pu, ^{238}U Stainless Steel	Axial and[b] Radial ^{25}f, ^{28}f, ^{28}c	Core Center	Core Center	✓	✓
2. III A (3) (Fuel Slump-Out, 1)	✓		"	"	"				
3. III B (3) (Fuel Slump-Out, 2)	✓		"	"	"				
4. IV A (4) (Fuel Slump-In, 1)	✓	Core Center	"	"	"[b]	Core Center	Core Center	✓	
5. V A (2)[c] (Blanket Collapse)			"	"	"				

[a] The location of foils etc., will be determined based on Monte Carlo code validation requirements.

[b] Detailed foil mappings will be done in these configurations. For the others a less detailed mapping will be made.

[c] This configuration might be deleted if time pressures so dictate.

However, the reactivity worth of intermediate compaction densities will be measured during the loading to full compaction. This should provide useful data for the validation of the neutronics portion of the SIMMER code.

The fuel slump-in configuration (Phase IV) has a calculated eigenvalue of 1.05 and presents problems with regard to adjustment to critical. The usual method of substituting blanket drawers for core drawers at the core/blanket interface would entail the removal of a large number of core drawers and significantly alter the leakage pattern from the core. Preanalysis results show that the adjustment to critical can be made by slumping to an axial height of 17.30 cm instead of 23.09 cm with very little adjustment to the core/blanket interface. The latter method has the advantage of much smaller operation time requirement and will be adopted.

The program plan was reviewed and approved by the Fast Reactor Critical Experiment Review Group of the Nuclear Regulatory Commission in June, 1977. An internal review was undertaken by the Applied Physics Division at ANL and the program was approved in July, 1977.

THREE-DIMENSIONAL CODE DEVELOPMENT FOR CORE THERMAL HYDRAULIC ANALYSIS OF LMFBR ACCIDENT UNDER NATURAL CONVECTION CONDTIONS (A2045)

A. Flow Stratification in a Pipe (W. T. Sha, H. M. Domanus and R. C. Schmitt)

Flow stratification in a pipe of 0.46 m diameter with 21.34 m long has been studied by using COMMIX code.[18] The effective viscosity of 0.07 is used in this study. Figure 12 presents a comparison between the calculated radial velocity distribution and the experimental data[19] in fully developed flow regime, the agreement is good. The forcing functions, i.e., inlet flow rate and inlet velocity employed in the calculation are shown in Fig. 13. The transient starts at 40 sec. and ends at 80 sec. (see cross hatch area of Fig. 13). Both fully developed velocity profile and uniform temperature are assumed throughout the pipe at time t = 0 sec. Figs. 14-18 presents the normalized temperature profiles of a veritcal plane passing the centerline along the x-axis (pipe length) at t = 0, 10, 20, 30 and 40 sec respectively. Radial velocity profiles at axial location x = 5.791 m are shown in Figs. 19-23 at t = 0, 10, 20, 30 and 40 sec respectively. Axial velocity distributions at t = 0, 10, 20, 30 and 40 sec are shown in Figs. 24-28 respectively. Figure 29 summarizes temperature distributions along the center line from top of the pipe to bottom. The above calculations was funded by ERDA under 189A CA055.

Based on this study it concluded that:

(1) Thermal buoyancy force can create appreciable secondary flow in radial direction (Figs. 20-23) and reverse flow in axial direction (Figs. 26-28), thus it significantly affects the hydraulic resistance.

(2) Large circumferential temperature gradients have been observed in this calculation (Fig. 29) thus it induces thermal stress.

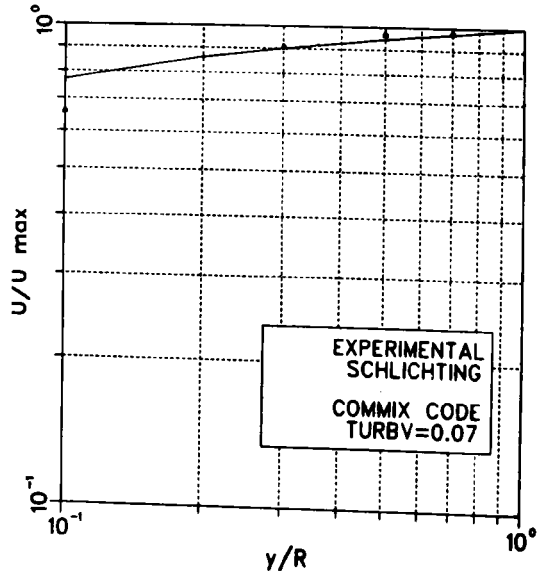

Fig. 12. Radial Velocity Profile ANL Neg. No. 116-77-537

1

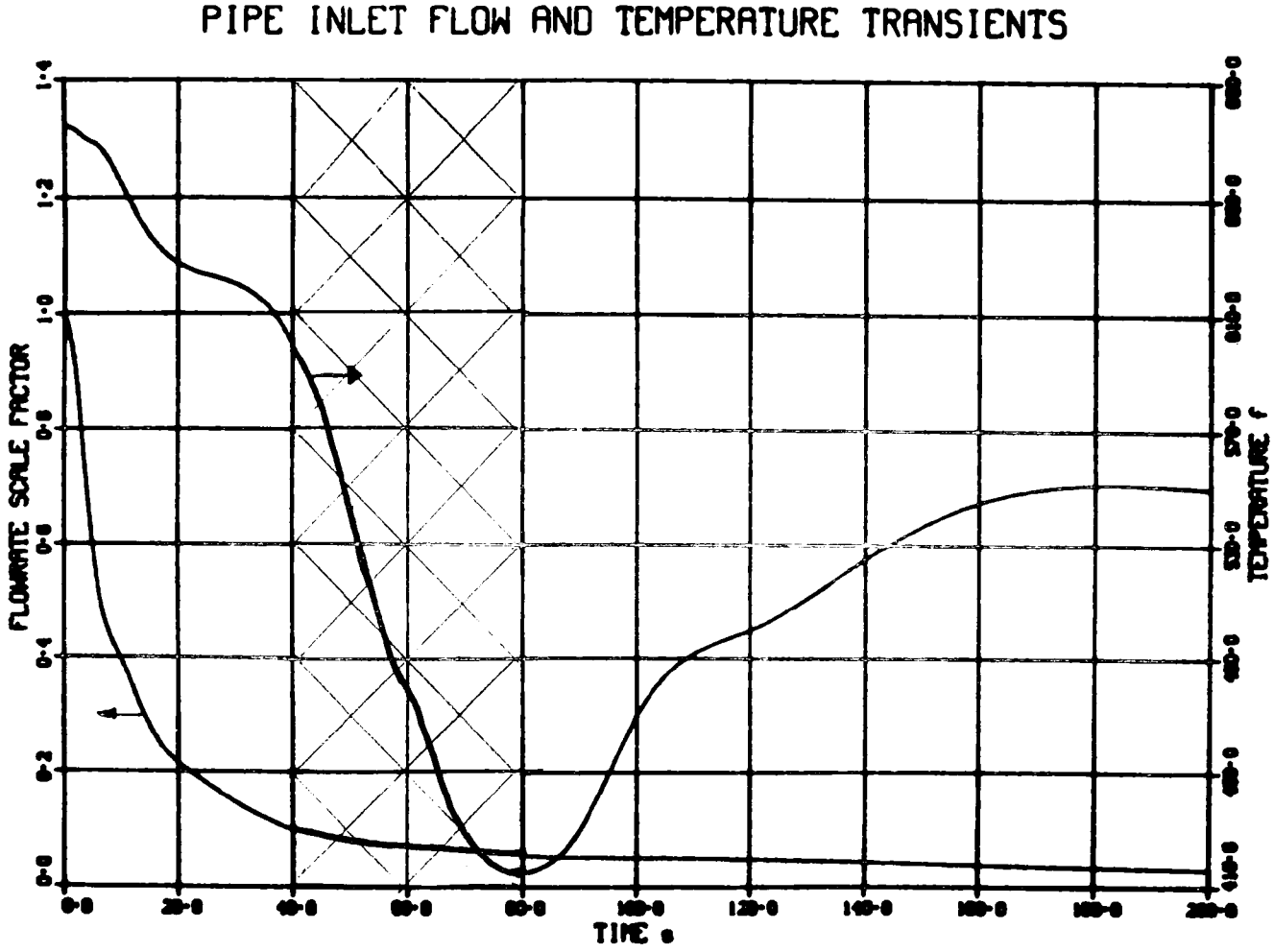

Fig. 13. Forcing Functions at Inlet of a Pipe ANL Neg. No. 116-77-557

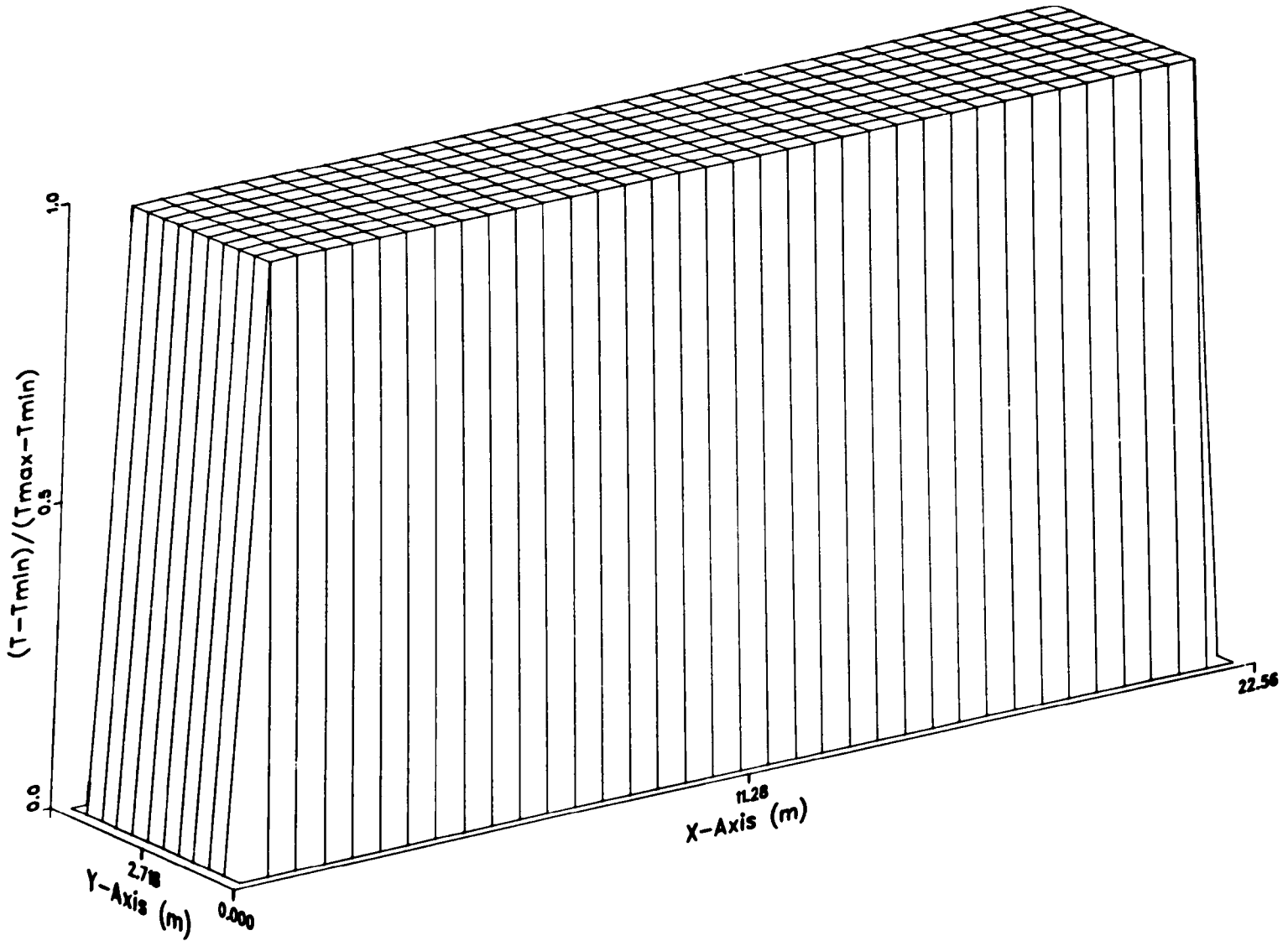

Fig. 14. Temperature Profile at t = 0 s ANL Neg. No. 116-77-558

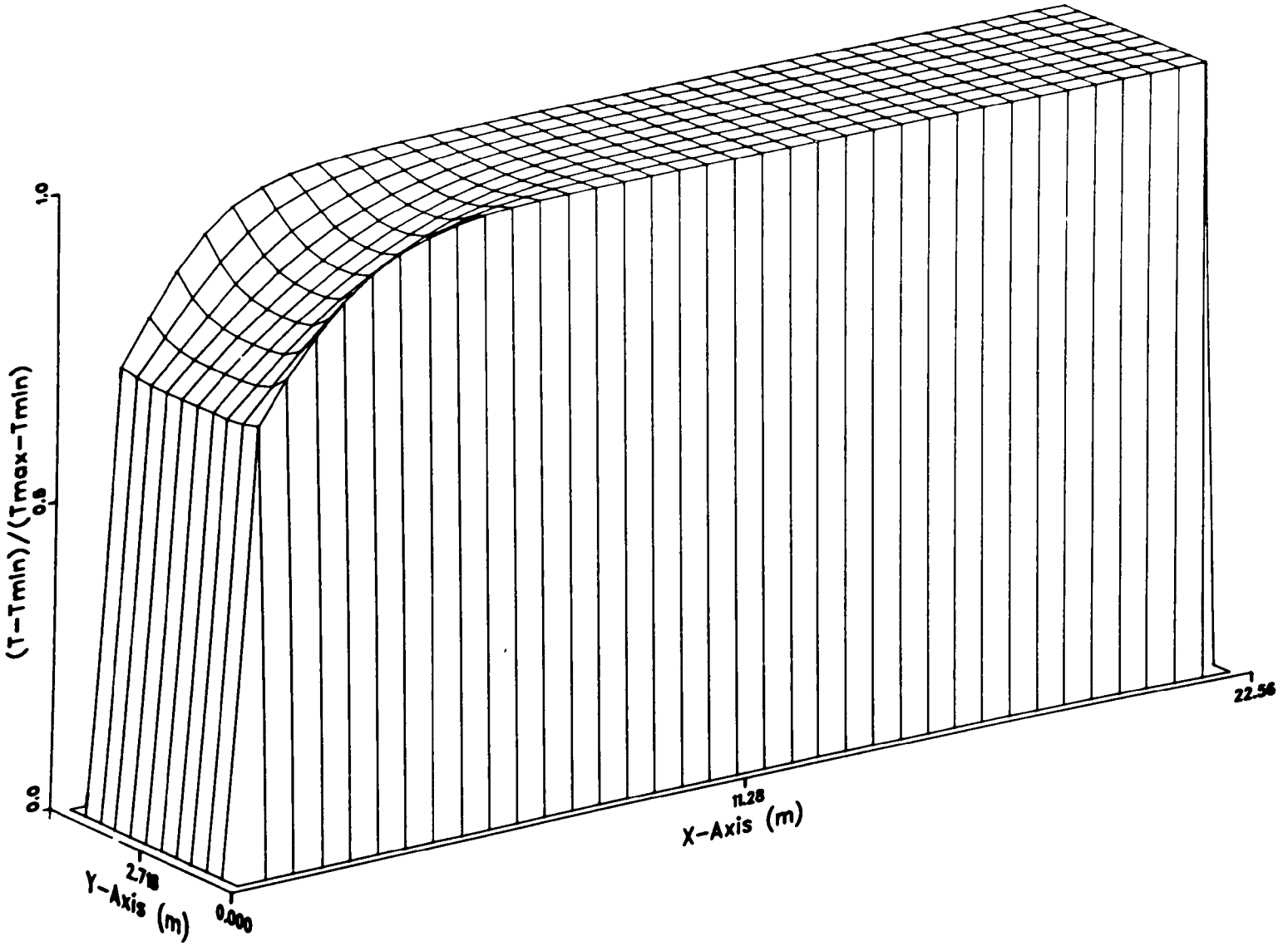

Fig. 15. Temperature Profile at t = 10 s ANL Neg. No. 116-77-559

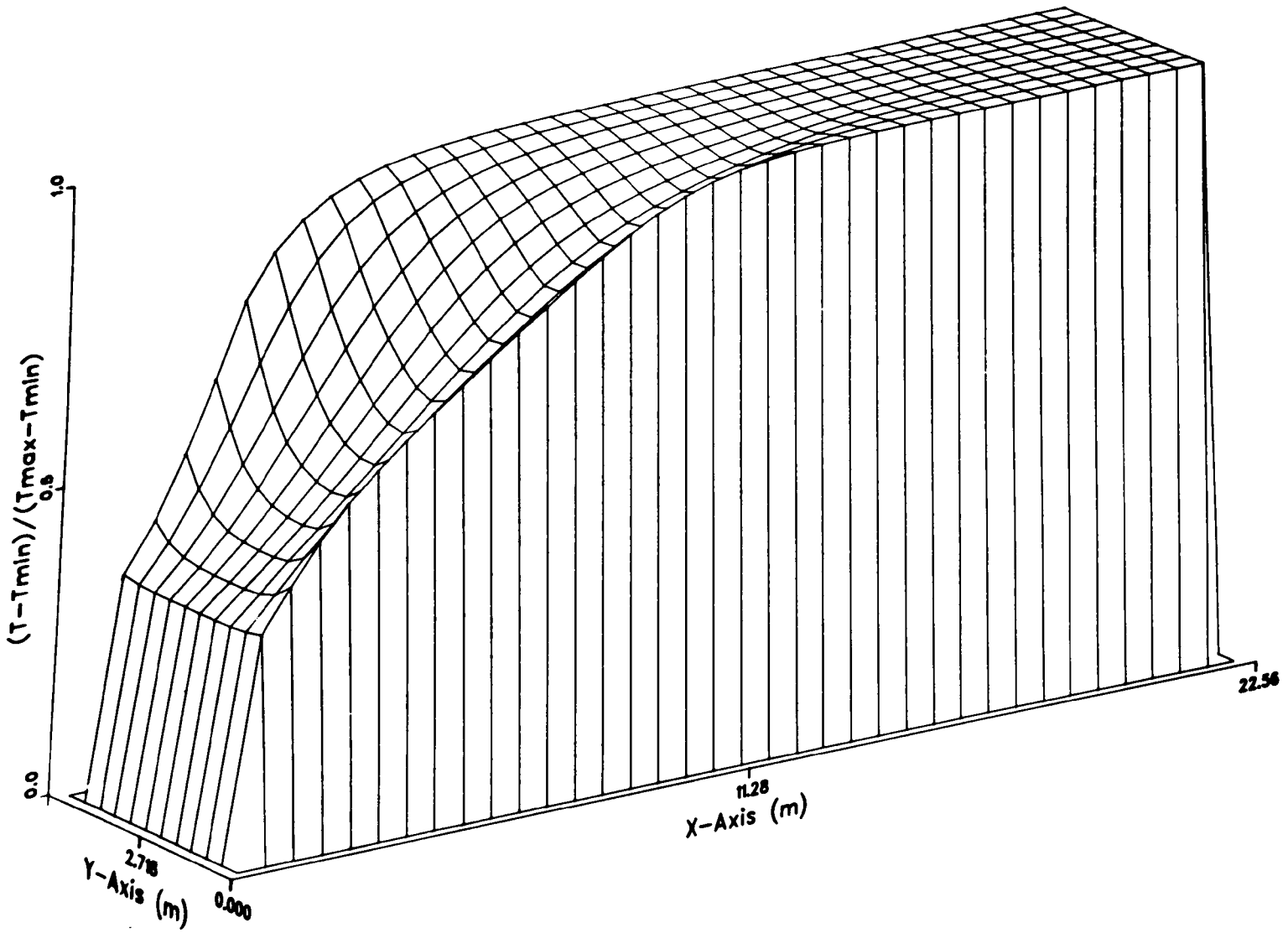

Fig. 16. Temperature Profile at t = 20 s ANL Neg. No. 116-77-560

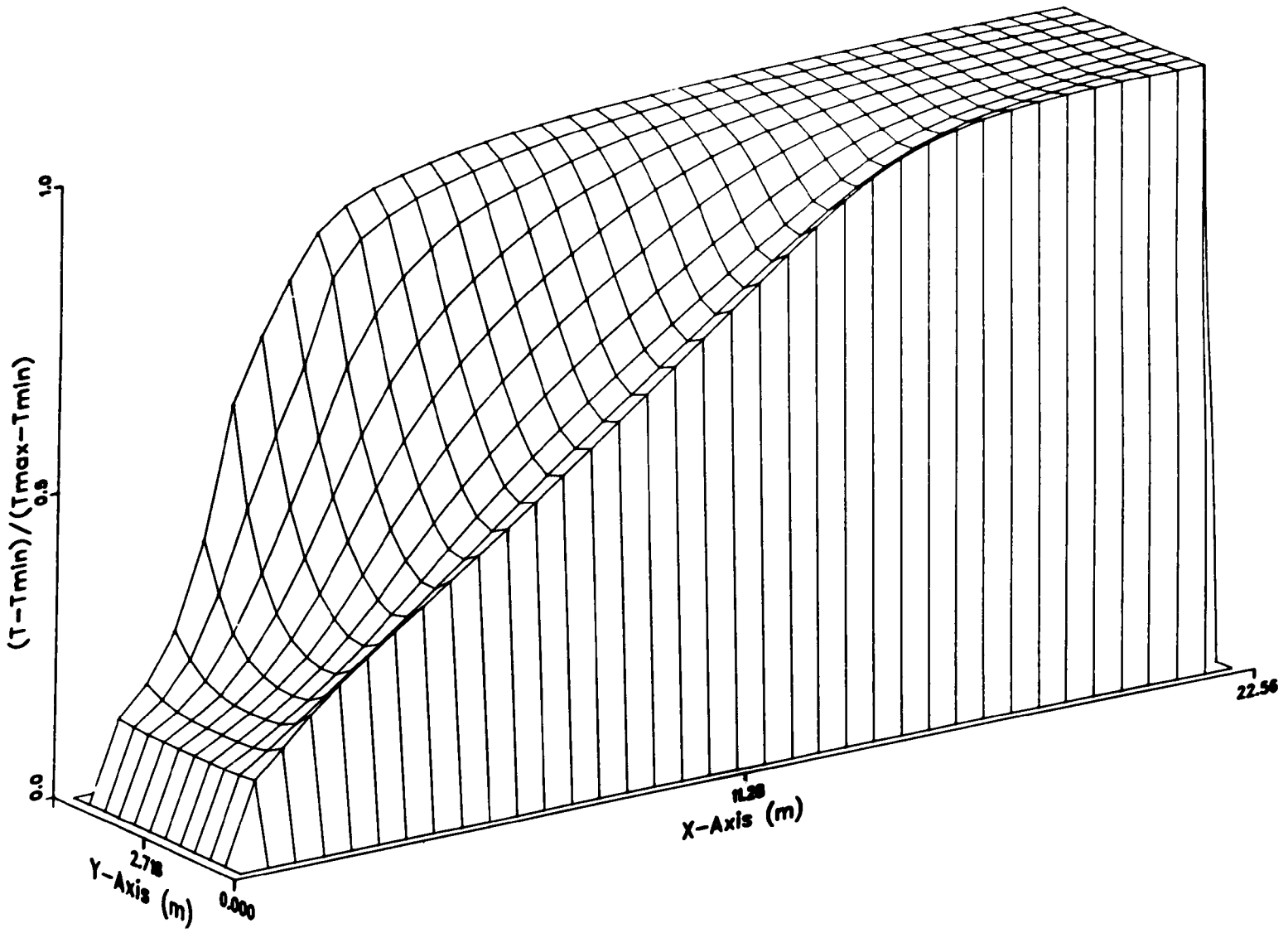

Fig. 17. Temperature Profile at t = 30 s ANL Neg. No. 116-77-554

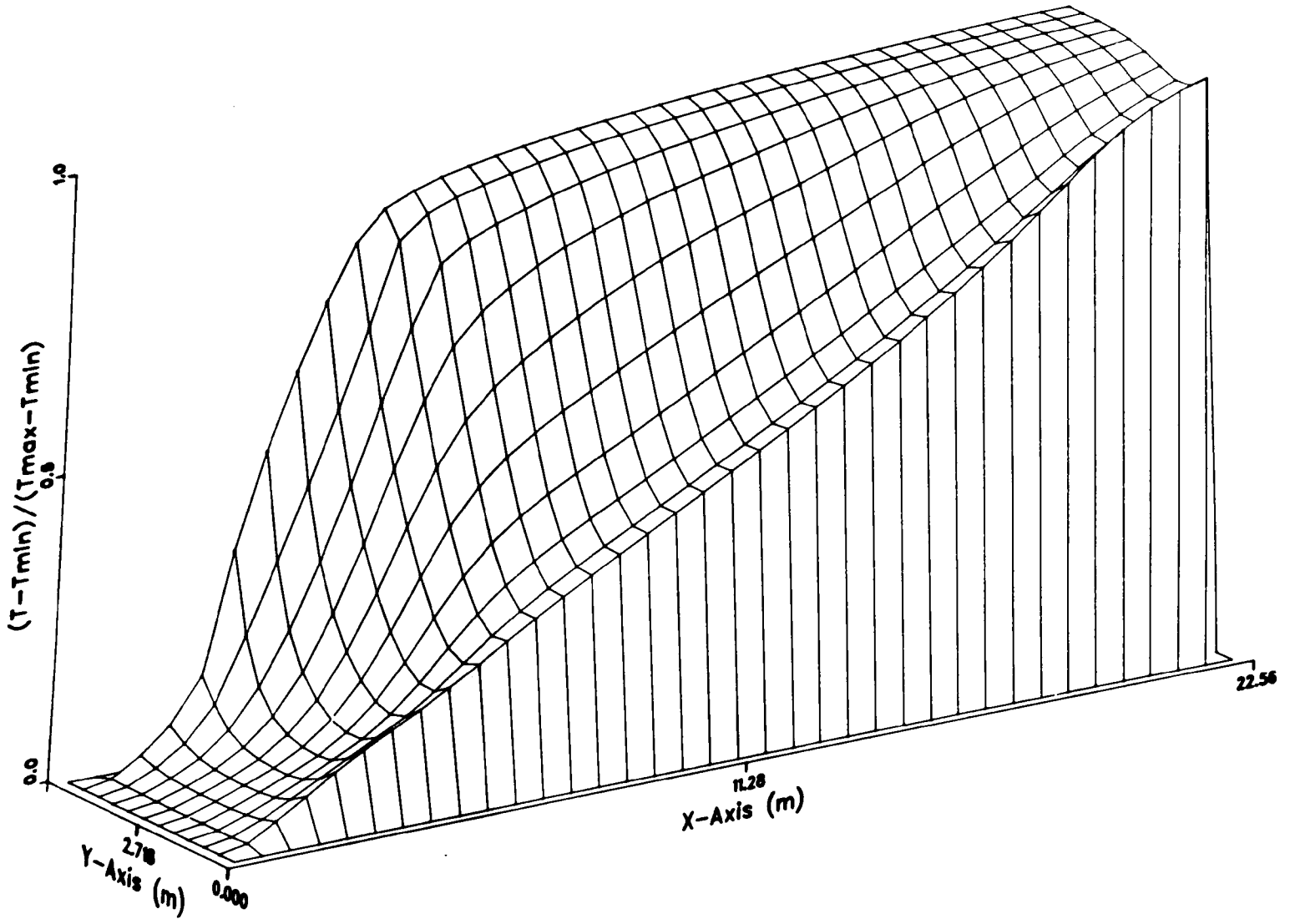

Fig. 18. Temperature Profile at t = 40 s ANL Neg. No. 116-77-553

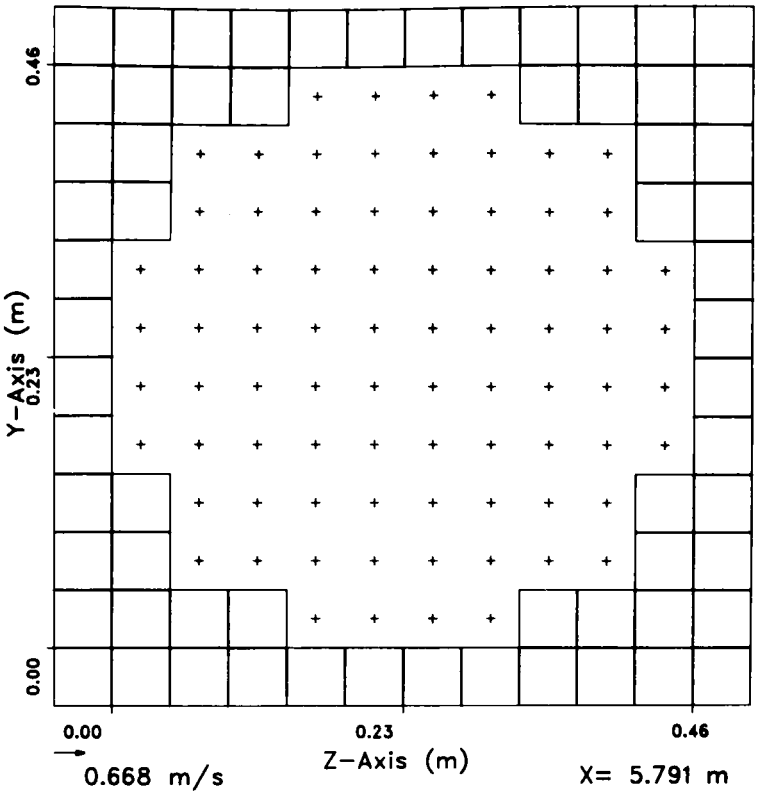

Fig. 19. Radial Velocity Distribution at t = 0 s ANL Neg. No. 116-77-541

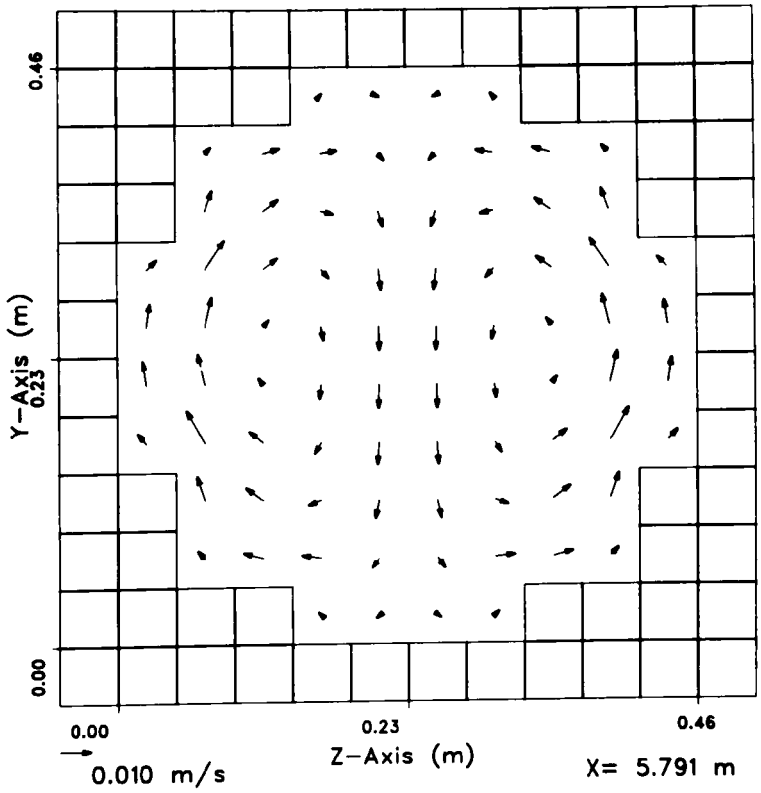

Fig. 20. Radial Velocity Distribution at t = 10 s ANL Neg. No. 116-77-543

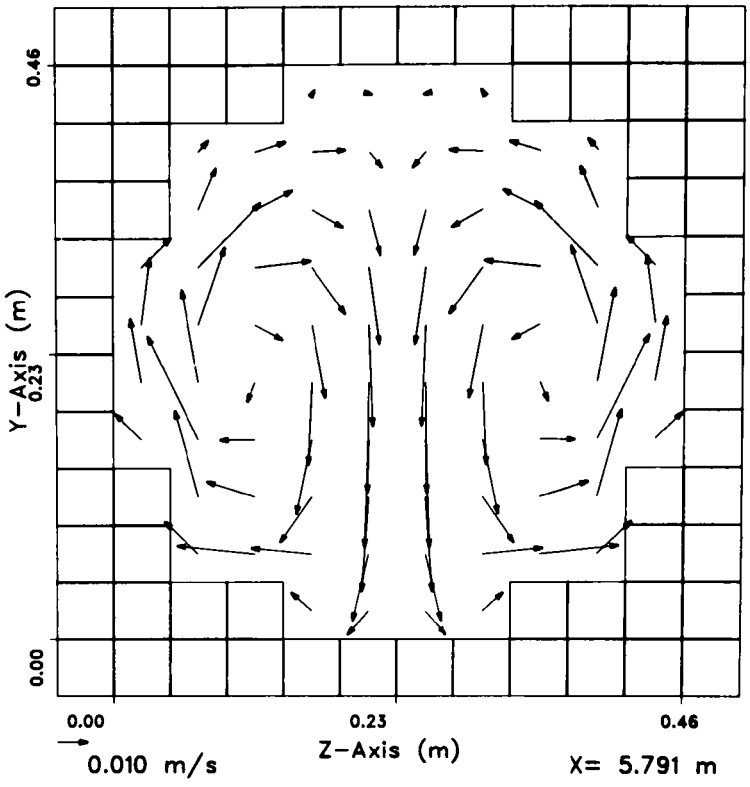

Fig. 21. Radial Velocity Distribution at t = 20 s ANL Neg. No. 116-77-542

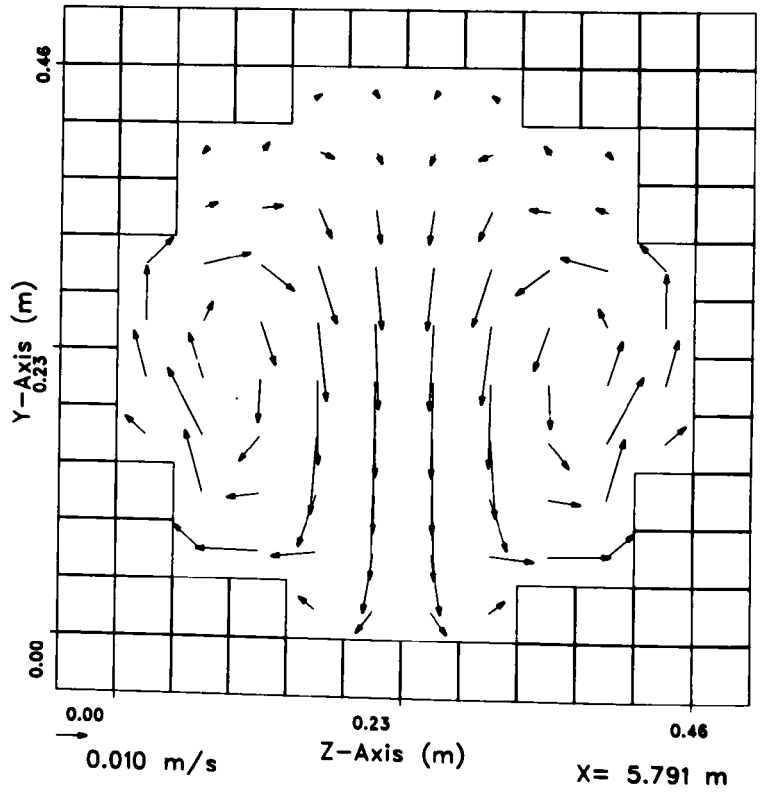

Fig. 22. Radial Velocity Distribution at t = 30 s ANL Neg. No. 116-77-548

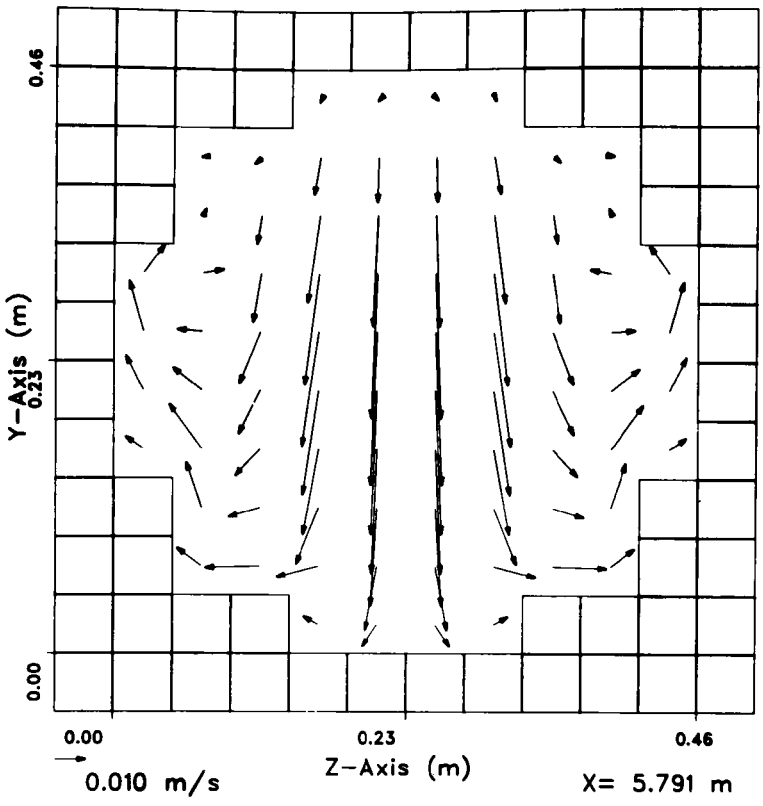

Fig. 23. Velocity Distribution at t = 40 s ANL Neg. No. 116-77-546

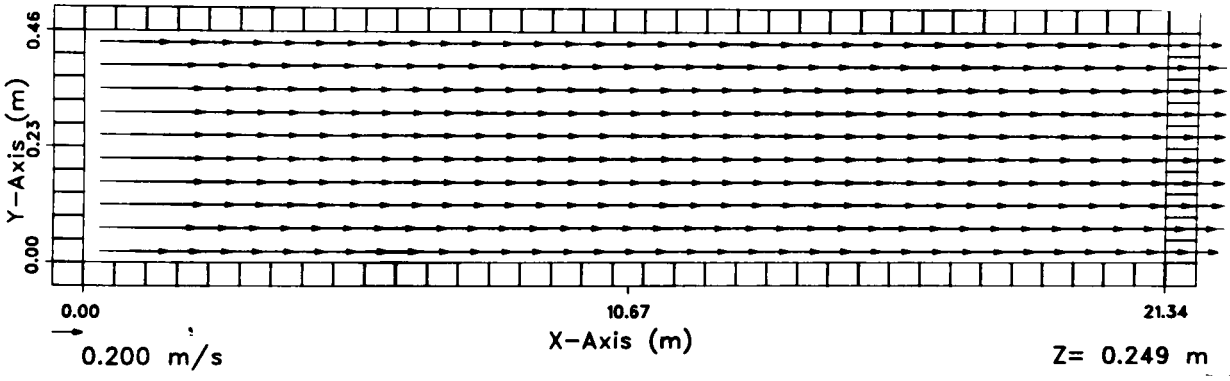

Fig. 24. Axial Velocity Distribution at t = 0 s ANL Neg. No. 116-77-547

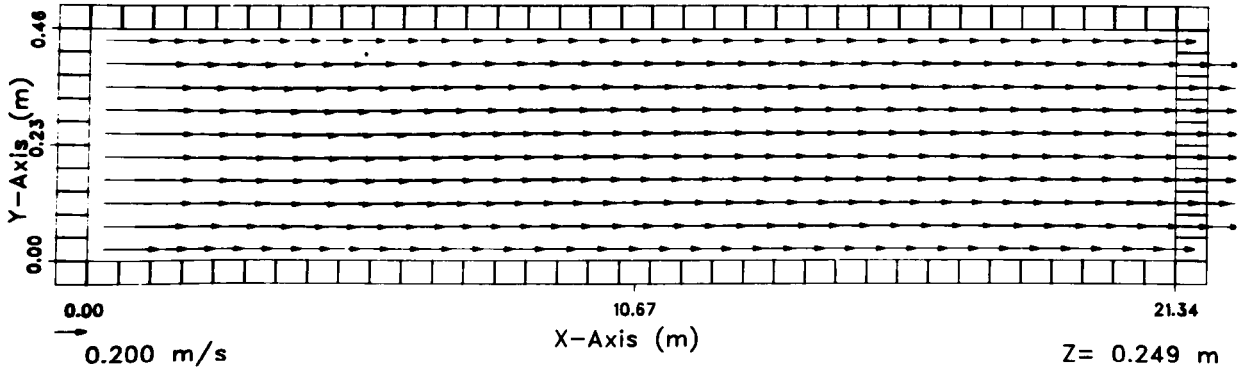

Fig. 25. Temperature Distribution at t = 10 s ANL Neg. No. 116-77-545

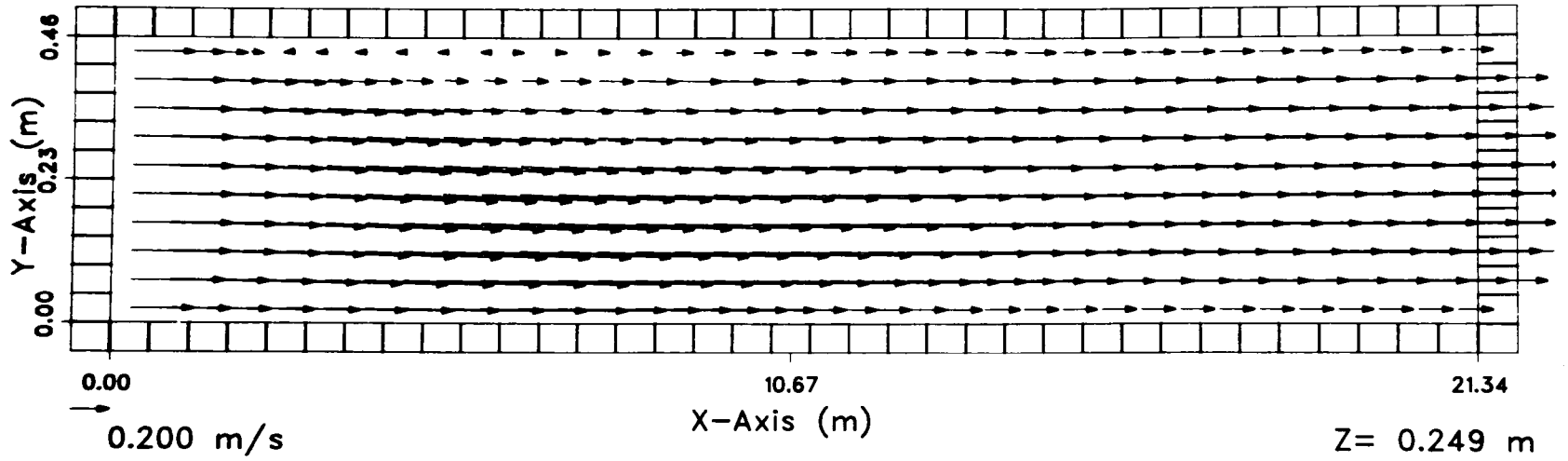

Fig. 26. Temperature Distribution at t = 20 s ANL Neg. No. 116-77-555

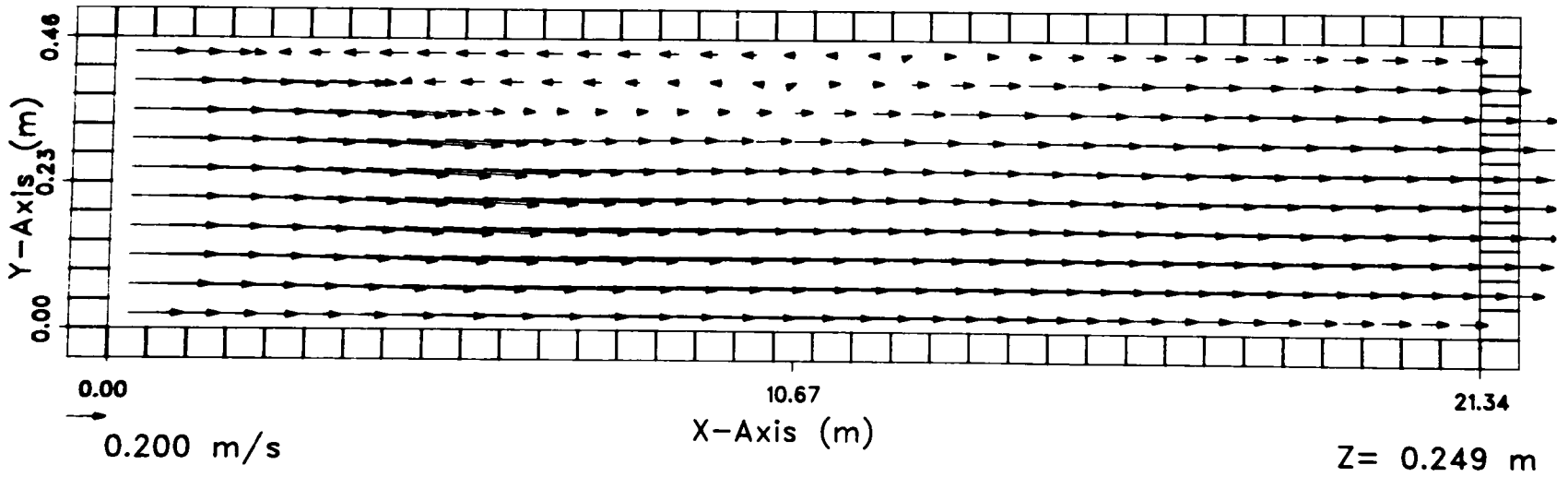

Fig. 27. Temperature Distribution at t = 30 s ANL Neg. No. 116-77-556

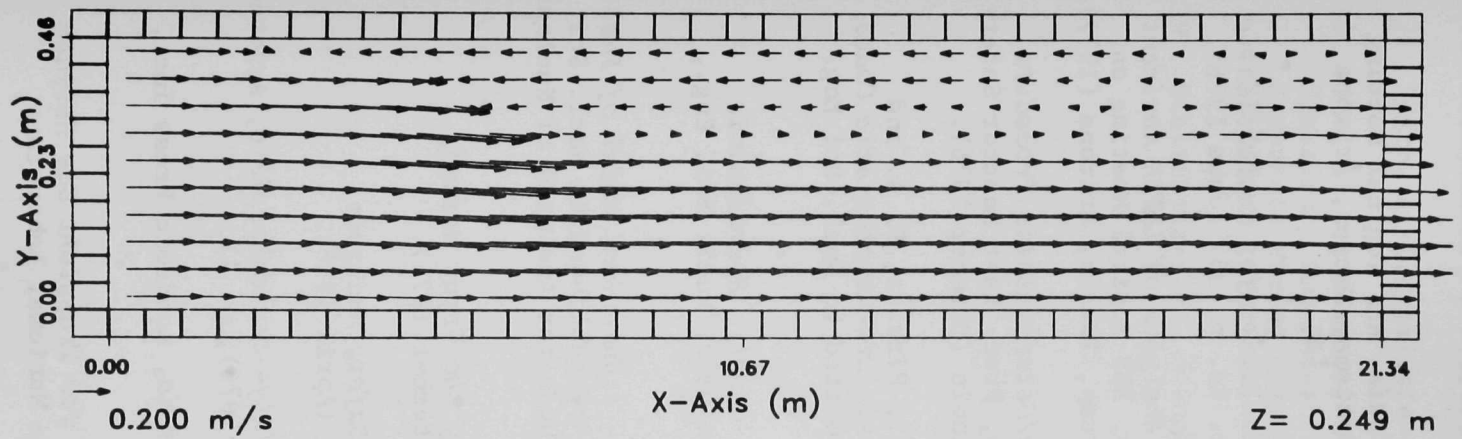

Fig. 28. Temperature Distribution at t = 40 s ANL Neg. No. 116-77-551

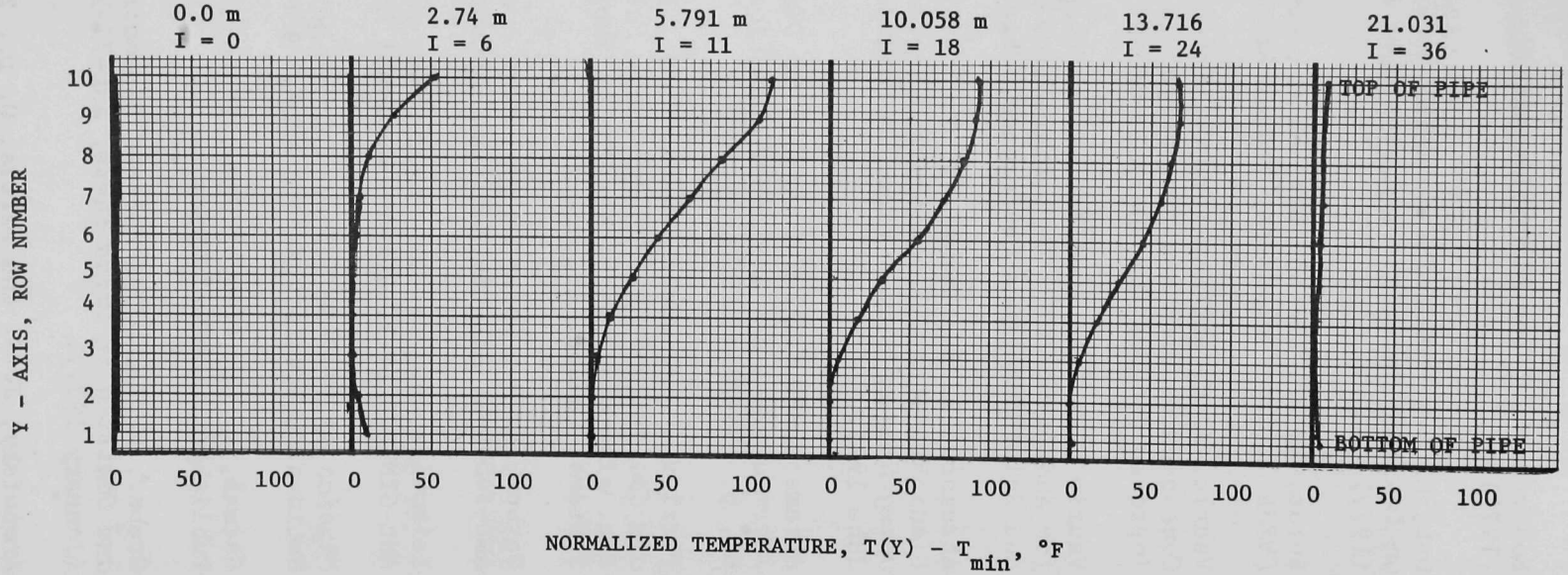

Fig. 29. Temperature Distribution at Various Axial Locations ANL Neg. No. 116-77-552

References

1. Boudreau, J., Los Alamos Scientific Laboratory, private communication (1977).

2. Ott, K. O., *Probabilistic LMFBR Accident Analysis,* ANS Topical Meeting on Improved Methods for Analysis of Nuclear Systems, Tucson, Arizona (1977).

3. Burns, R. D., III and Ott, K. O., *Accident Simulation for Probabilistic LMFBR Safety Evaluation,* Trans. Am. Nucl. Soc. 23, p. 337 (June 1976).

4. Vaurio, J. K. and Mueller, C., *Probabilistic Analysis of LMFBR Accident Consequences with Response Surface Techniques,* ANS Topical Meeting on Improved Methods for Analysis of Nuclear Systems, Tucson, Arizona (1977).

5. Vaurio J. K. and Mueller, C., *A Probabilistic/Deterministic Procedure for Analyzing LMFBR Core Disruptive Accidents,* Proc. Fast Reactor Safety and Related Physics Conference, Chicago, Illinois (October 1976).

6. Abramson, P. B., Hummel, H. H., Gelbard, E. M., Pizzica, P. A. and Sienicki, J. J., *Probabilistic Accident Analysis with Mechanistic Codes Using Stochastically Variable Parameters,* submitted to Nucl. Sci Eng. June 1977.

7. Abramson, P. B., *FX2-POOL - A Two Dimensional Coupled Hydrodynamic Thermodynamic and Neutronic Model for HCDA Analysis,* Nucl. Sci. Eng., 62, p. 195-214 (1977).

8. Pizzica, P. A. and Abramson, P. B., *EPIC-FCI - A Numerical Model of Fuel and Coolant Motions Following Pin Failure,* to be published in Nucl. Sci. Eng. also ANS Topical Meeting on Improved Methods for Analysis of Nuclear Systems, Tucson, Arizona (1977).

9. Garbow, B. S., *Solution of Linear Equations by the Crout Method,* ANL-F454S-2, Argonne National Laboratory (September 1975).

10. Leibowitz, L., et. al., *Properties for LMFBR Safety Analysis,* ANL-CEN-RSD-76-1, Argonne National Laboratory (April 1976).

11. *Physics of Reactor Safety: Quarterly Report, July--September 1976,* Argonne National Laboratory Report ANL-77-9 (December 1976), p. 11.

12. Carman, P. C., *Flow of Gases Through Porous Media,* Academic Press Inc., Publishers, London (1956).

13. Gruber, E. E., *A Generalized Parametric Model for Transient Gas Release and Swelling in Oxide Fuels,* ANL-77-2, Argonne National Laboratory (January 1977).

14. Aronofsky, J. S. and Ferris, O. D., *Transient Flow of Non-Ideal Gases in Porous Solids - One-Dimensional,* J. of Applied Physics, 25, p. 1289 (1954).

15. Kato, W. Y. et al., *Final Safety Analysis Report on the Use of Plutonium in ZPR-6 and -9*, ANL-7422, Argonne National Laboratory (1970).

16. Wood, P. M., private communication (October 1976).

17. Smith, L. L., private communication (May 1977).

18. Sha, W. T., Domanus, H. M. and Schmitt, R. C., *COMMIX-A Three-Dimensional, Transient, Two-Phase Flow with Non-Equilibrium Temperature and Reactor Componets Mixing Computer Program*, Argonne National Laboratory, to be published 1978.

19. Schlichting, H., *Boundary Layer Theory*, McGraw Hill, NY (1955).